# Modification of Wide Bandgap Semiconductors for Visible Light Driven Hydrogen Generation

By

Sujoy Saha


A Dissertation submitted

in partial fulfilment of the requirements for the degree

BS-MS Dual Degree Programme

In

Chemistry

Supervised by

Prof. C.N.R. Rao, *FRS*

Jawaharlal Nehru Centre for Advanced Scientific Research, Bangalore

Indian Institute of Science Education and Research, Pune

March 2015

# Certificate

This is to certify that this dissertation entitled "**Modification of Wide Bandgap Semiconductors for Visible Light Driven Hydrogen Generation**" towards the partial fulfilment of the **BS-MS dual degree** programme at the Indian Institute of Science Education and Research (IISER), Pune represents original research carried out by **Sujoy Saha** at Jawaharlal Nehru Centre for Advanced Scientific Research (JNCASR) under the supervision of **Prof. C.N.R. Rao, *FRS*,** *National Research Professor and Honorary President & Linus Pauling Research Professor* during the academic year **2014-2015**.

.....

Prof. C. N. R. Rao

(Supervisor)

Dated: 24.03.2015

# Declaration

I hereby declare that the matter embodied in the report entitled "**Modification of Wide Bandgap Semiconductors for Visible Light Driven Hydrogen Generation**" are the results of the investigations carried out by me at the Jawaharlal Nehru Centre for Advanced Scientific Research (JNCASR), under the supervision of Prof. C.N.R. Rao, *FRS* and the same has not been submitted elsewhere for any other degree.

Sujoy Saha

Sujoy Saha

Dated: 24/03/2015

# ABSTRACT OF THE DISSERTATION

## Modification of Wide Bandgap Semiconductors for Visible Light Driven Hydrogen Generation

By
Sujoy Saha

*As fossil fuels are likely to be exhausted in the near future, Hydrogen, a new cheap, renewable and non-polluting energy, has been considered as next-generation energy carrier. Photocatalytic $H_2$ generation, as practiced in the present dissertation, is the central process to achieve the goal of $H_2$ production from renewable resources. Photocatalytic activities for $H_2$ production, using some wide band gap semiconductors have been demonstrated successfully, but under UV light irradiation. Hence, to utilize the sunlight more efficiently, new visible light active photocatalysts need to be developed. While development of noble visible light active photocatalysts is in progress, chemical modifications of UV-active wide bang gap semiconductors to extend the photoactivity into visible region, have become a promising way. Several strategies, such as, (i) element doping, (ii) Forming Solid Solution, (iii) Interfacial Hetero-junction, (iv) Plasmonic modification, and (v) Surface Catalyst Decoration have been proposed. The above strategies have been adopted in the current project, to use chemically modified nanostructures of wide band gap semiconductors, such as ZnS, ZnO and $TiO_2$, to demonstrate significant advancement in the photocatalytic water splitting. The first effort concerns about band engineering by doping; P,Cl- and N,F-codoping in ZnS (and CdS) reduces the band gap and could be used for visible light induced water splitting*. Then ZnO was used to make a solid solution with CdO to narrow the band gap and tried to use in visible light induced $H_2$ generation. ZnO and $TiO_2$ was sensitized with CdS and morphology dependent $H_2$ generation was demonstrated by ZnO($TiO_2$)/CdS heterostructure*. An unsuccessful attempt was made to do plasmonic modification of $TiO_2$ by $ReO_3$, which shows SPR in visible region, but could not be used in water splitting due to instability in water. Lastly, CuS cocatalyst loaded ZnO has showed $H_2$ evolution by visible light driven water splitting.*

* Based on this project, two manuscripts have been submitted to *Angew. Chem. Int. Ed.*, 2015, and *Chem Phys Lett., 2015.*

# Acknowledgments

Time flies. Eight months have passed, since I started my research work at JNCASR. Now, I take immense pleasure for the chance to thank the people who have helped me and enriched my experience during this time.

First and foremost, I would like to thank my supervisor Prof. C.N.R. Rao. He not only introduced me to the fascinating field of Water Splitting but also has helped me with his invaluable guidance and constant encouragement. He is a person of immense enthusiasm and wisdom. It is a rich and wonderful experience to work under his guidance, which will motivate and benefit me for the rest of my life.

I would like to thank my collaborators Dr. P Chithaiah, Mr S. R. Lingampalli and Mr Anand Roy for helping me to carry out experiments and provide me the deep insights into the research works. Also, I would like to thank all my present and past labmates.

In this chance, I would like to thank my former research supervisor Dr. Angshuman Nag for being such a good 'friend, philosopher and guide'. Without his help and encouragement I could not be prepared for future endeavour.

My sincere appreciation also goes to IISER Pune, for providing me such an opportunity to start my research, as well as academic experience.

Over this period of time, I have been fortunate to have such good friends; Sunitadi, Anaranya, Subhojit, Malabika, Badri, Abhijit, Akash, Abhirup, Raktim, Manoj, Sudip, Moumitadi, Manjeetda, Arun, Aniruddh, and last but not least, Uttamda; I would like to thank them all for having a wonderful time at JNCASR and/or NVSH.

Finally and most importantly, I would like to dedicate this work and effort to my Family for everything they have done for me. Without their love, encouragement and support, I could not go forward with science and research.

There are many others who deserve my thanks. Thanks to them also.

# Table of Contents

# List of Figures and Tables

## Chapter 1



## Chapter 2



## Chapter 3

## Chapter 4



## Chapter 5



## Chapter 6



## Chapter 7

# Chapter 1

## Towards A Sustainable Future: Introduction to Photocatalytic $H_2$ generation by visible light driven water splitting

*This chapter addresses the question raised over current energy crisis issue. Shortage of energy sources have been the bottle-neck of survival, and hence direct utilization of solar energy is the headstone for mankind since decades. Hydrogen is being considered as an alternative energy in near future, since fossil fuels are about to exhaust. Fundamentals of Photocatalytic $H_2$ generation has been discussed. A section is also devoted about why and how it is necessary to utilize of most part of solar spectrum, i.e., visible light driven water splitting. Drawbacks of current semiconductor photocatalytic systems have been specified in a section, followed by the strategies adopted to solve those problems aiming efficient $H_2$ generation on semiconductor photocatalyst.*

# 1.1 Introduction

## 1.1.1 Dirty past, clean future?

Think back for a second, only about two hundred years ago, that was a time when there was no vehicle, no electricity, no industry, no…; but a human race, equilibrated with earth. Then, ever since the Industrial Civilization started, mankind started booming, sitting in the chariot of science and technology, even, have touched the soil of the moon, but what was ignored, is losing soil under the feet in earth itself, rapidly exploiting the fossil fuels. Standing on the precipice of an extinction level crisis, human is seeking for an alternative renewable clean energy source, looking at sun, the ultimate source of life itself.

Efficient utilization sunlight could alleviate the energy crisis, as the solar energy illuminating the surface of the Earth ($1.3 \times 10^5$ TW) dwarfs the current global human energy consumption ($1.6 \times 10^1$ TW in 2010). Hence, developing an artificial system, which can mimic the natural photosynthesis to absorb and convert solar energy directly into storable and usable energy resources, has received much attention. Photocatalytic water splitting, in which solar energy is used to drive redox reactions to produce hydrogen energy, is the primal procedure to accomplish this aim.

## 1.1.2 Introduction to Photocatalytic Water Splitting:

The word “Photocatalysis” is Greek in origin, means phos or light and katalyo or break apart. However direct decomposition of water by light is not possible, because water is transparent to visible light, except only with the irradiation shorter than 190nm (deep UV light). To drive photocatalytic water splitting, a potential of at least 1.23 V is needed, equivalent to the energy irradiance of ~1000 nm. If we can harvest sunlight effectively in a photocatalytic system, it should be possible to achieve water splitting.

The first photocatalytic water splitting was demonstrated by Honda and Fujishima in 1972, in a photoelectrochemical (PEC) cell [1]. Upon illumination, the n-type semiconductor $TiO_2$ photoanode will absorb UV light to generate electron-hole pairs. If an anodic potential is applied through an external circuit, these photoexcited electrons ($e^-$) migrate through the circuit to reach the Pt counter electrode, and reduce water into $H_2$. The holes ($h^+$) left behind, diffuse to the surface of $TiO_2$ and oxidize $H_2O$

to form $O_2$, see in Fig. 1.1. The reaction occurs in the electrodes are:

Photoanode: $H_2O + 2h^+ \rightarrow 2H^+ + 1/2O_2$ $E^0_{ox} = -1.23$ V vs SHE (1.1)

Cathode: $2H^+ + 2e^- \rightarrow H_2$ $E^0_{red} = 0$ V vs SHE (1.2)

Following the Nernst equation, at least 1.23V will be required to drive the water splitting. To fulfil this energy need, the semiconductor electrode must absorb photon energies more than 1.23 eV to drive solar water splitting. However, for sustainable photocatalytic water splitting without applying external bias, a bandgap larger than1.23 eV is necessary but not enough.

In photocatalytic water splitting process, photon energy, is used to break the bonds in water and is converted to the chemical energy of $H_2$, giving $H_2$ and $O_2$ as final products (Eq. 1.6), known as 'artificial photosynthesis'. Thermodynamically this process is a typical "uphill reaction" and involves a large positive Gibbs free energy change ($\Delta G^0$= 238 kJ $mol^{-1}$).

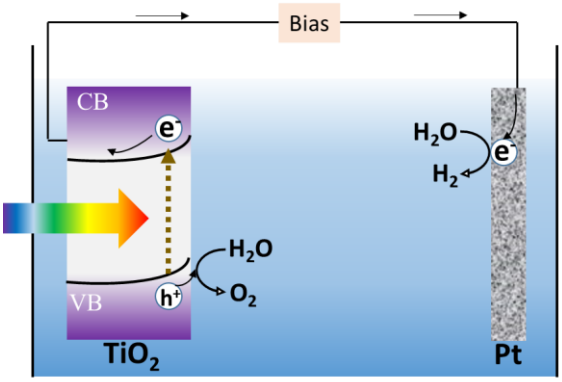


Fig. 1.1. Photocatalytic water splitting in PEC based on $TiO_2$ photoelectrode.

To overcome this uphill task, artificial photosynthesis offers desired efficiency and follows the principles similar to natural photosynthesis. It consists generally a photon-absorbing site and a catalytic site, with a hole and electron transfer pathway joining the two. It can be employed in a single- or two- step process.

In one-step process, the photon absorber is connected with an electron donor on one side and/or an electron acceptor on the other. A semiconductor or a dye can act as the photon absorber, which absorbs photons with energy exceeding the HOMO–LUMO gap of the dye or band gap of the semiconductor, generating an electron–hole pair which take part in redox reactions, see Fig. 1.2a.

Alternatively, in the two-step process, two photon absorbing sites are connected in series. The rest of the mechanism are similar to the single-step process, see Fig. 1.2b. A reversible redox couple is used as the electron transfer relay. On one absorber, $H_2O$ gets reduced to give $H_2$ along with oxidation of reduced redox shuttle whereas on other absorber the oxidized redox mediators get reduced with oxidation

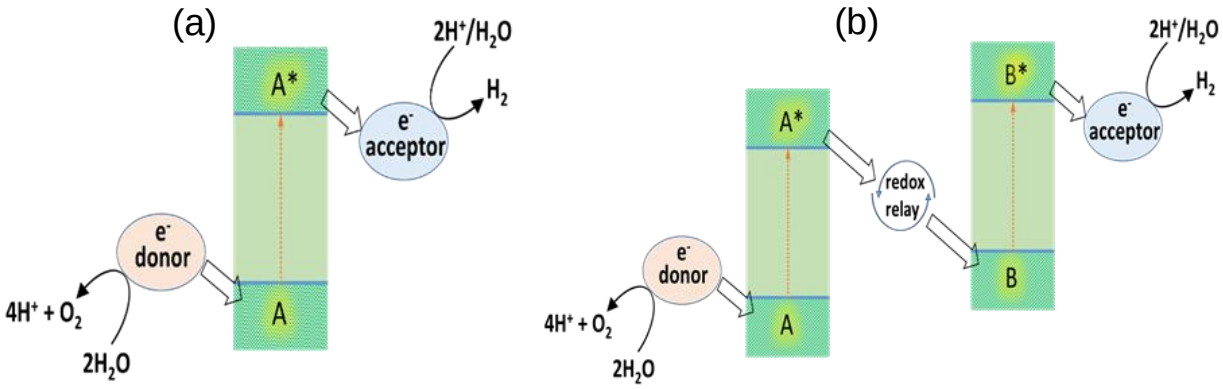


Fig. 1.2. (a) One-step and (b) two-step process of artificial photosynthesis.

of $H_2O$ to $O_2$ concurrently. The two-step system is named as the ‘‘Z-scheme’’ after the natural photosynthesis because of the similarity in the photogeneration of electron and hole pairs and charge transfer processes and uses two photon to generate an exciton.

### 1.1.3 Thermodynamics of Photocatalytic Water Splitting

The basic principles of the overall water splitting on a semiconductor particulate is illustrated schematically in Fig. 1.3, which is essentially similar to a water-splitting PEC cell. Upon illumination of photon, electron-hole pairs are generated, which can cause surface redox reactions, if the charge injections into the reactants are thermodynamically favourable. To achieve the overall water splitting, the CB and VB of semiconductors must straddle the electrochemical potentials of $E_o(H^+/H_2)$ and $E_o(O_2/H_2O)$ in such ways, that the photo-generated electrons and holes get enough electrochemical potential to drive water splitting without external bias. Therefore, to drive the reaction, thermodynamically the minimum photon energy requirement is 1.23 eV. However, an activation barrier is there, see the following section, and hence a photon energy greater than the band gap is necessary to drive the overall water-splitting reaction efficiently. Hence, amongst lots of materials, which own suitable band gap potentials, few can be used as a photocatalyst.

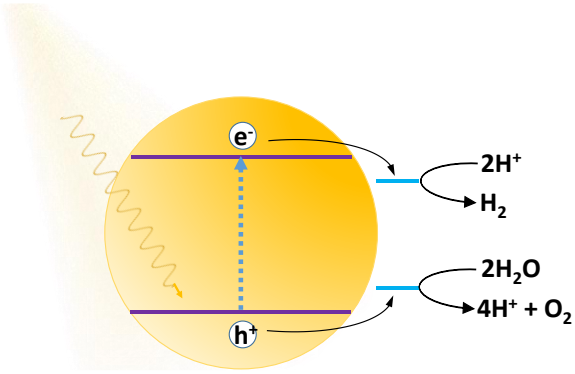


Fig. 1.3. Principle of the photocatalytic water splitting.

### 1.1.4 Working Mechanism of Photocatalytic Water Splitting

As illustrated in Fig. 1.4, the overall water splitting on a semiconductor photocatalyst particulate involves three key steps:

(i) Absorption of photon having energy higher than the band gap by the photocatalyst material and photoexcitation of electron in the VB to the CB, leaving holes behind in the VB. An exciton, generated in the bulk, is indicated by star symbol.

$$h\nu \rightarrow e^- + h^\bullet \qquad (1.3)$$

(ii) Separation of photoexcited charge carriers and migration to the surface active sites without recombination.

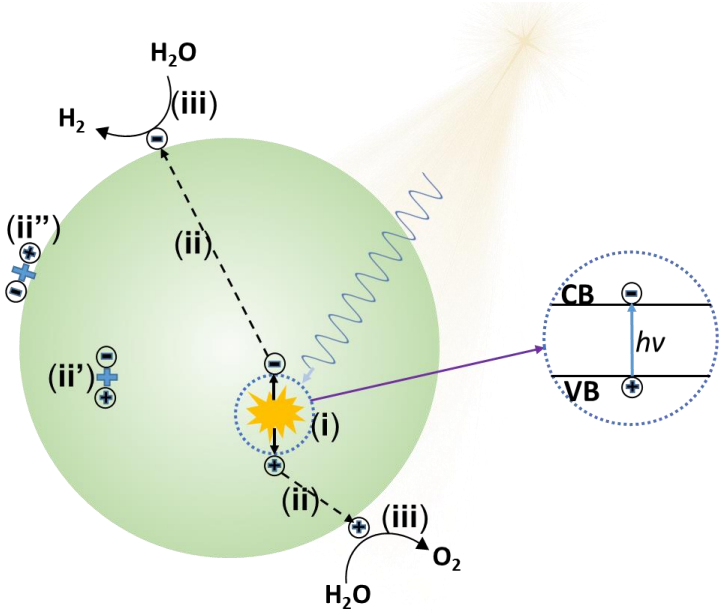


Fig. 1.4. Processes occurs in Photocatalytic water splitting.

(iii) Surface redox reactions, i.e., oxidation of adsorbed species by the holes

$$2H_2O_{(aq)} + h^\bullet \rightarrow 2H^+_{(aq)} + \tfrac{1}{2}\, O_{2(gas)} \qquad (1.4)$$

and reduction of protons by electron.

$$2H^+_{(aq)} + 2e^- \rightarrow H^2_{(gas)} \qquad (1.5)$$

The overall reaction is, $2H_2O_{(liq)} + h\nu \rightarrow 2H_{2(gas)} + O_{2(gas)}$ (1.6)

This reaction takes place when the energy of the photon absorbed by the semiconductor photocatalyst exceeds the threshold energy $E_t$,

$$E_t = \frac{\Delta G_o}{2N_A} \qquad (1.7)$$

Where $\Delta G^o$ is the standard free enthalpy (per mole) of Eqn. 1.3 = 238 kJ/mol and $N_A$ is the Avogadro's number = $6.023 \times 10^{23}$ $mol^{-1}$

Then we get, $E = h\nu = 1.23$ eV (1.8)

According to Eq. 1.7, photocatalytic water splitting is possible only when the semiconductor absorbs photon having energy of 1.23 eV or more.

However, in practice, the photon energy needs to be larger than the 1.23 eV, since there is an activation barrier for the surface chemical reactions that evolve $H_2$ and $O_2$ and charge transfer process between the photocatalyst and water molecules and for energy loss due to polarization within PEC and the potential loss for the resistance of electrode and contact. The energy loss estimated to be ~0.8 eV; therefore, the practical limitation of the photons to use for water splitting is ~2.0 eV.

## 1.2 Scope of the Current Study

### 1.2.1 Present Drawbacks of Photocatalysts

Currently, the efficiency of energy conversion in semiconductor photocatalytic water splitting is still suffering for low activity, the reasons being:

***(1) Recombination of photogenerated excitons and Photocorrosion:***

The greatest part of the excitons recombines before they can undergo photocatalytic reaction. See Fig. 1.4, processes ii'' and ii' denotes electron-hole recombination at the surfaces and bulk. The charge separation and redox reactions must proceed within the life-times of the excitons for successful water splitting. Fig. 1.5 depicts an energy diagram of trap states. These states come from the vacancies and defects in the crystal and offers new localized energy states that are not available in perfect lattice. Moreover, the surface can also renders a high density of energy states, since it is an abrupt discontinuity from lattice periodicity. These energy states act as traps for electrons, producing shorter exciton lifetime.

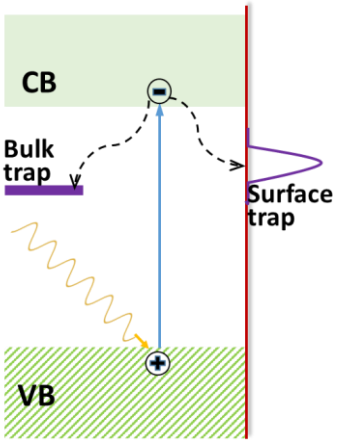


Fig. 1.5. Surface and bulk electron trap states for recombination.

One more demerit comes from the photogenerated holes, is photocorrosion. Rather than oxidizing $H_2O$, the holes corrodes the material itself.

***(2) Fast backward reaction:***

Recombination of $H_2$ and $O_2$ into $H_2O$ is a downhill process, and happens

easily. Hence, in the photocatalytic water splitting process, the reaction yields are, however, rather low, due to the recombination of the liberated gases at the surface.

***(3) Inability to utilize visible light:***

The biggest drawback of current photocatalytic systems, is that only UV light can be utilized for $H_2$ production, because of the wide band gap of well-studied semiconductors. Indeed only the photons of energy equal to or larger than band gap can be absorbed and used for conversion. Since the UV light accounts for only 4% of the solar spectrum, whereas the visible light comprises about 50%, the inaccessibility to employ visible light limits the efficiency of solar light driven photocatalytic $H_2$ production. This will be discussed in Chapter 2 in details.

### 1.2.2 Solutions considered

The above mentioned problems are tried to deal with following strategies:

**(1**) Using nanostructured semiconductors can inhibit the recombination of the photogenerated excitons greatly, by shortening charge carrier diffusion distance, and increasing electrolyte accessible surface area to take part in surface reactions.

Throughout this project, we will use nanosized photocatalyst particulate.

Adding electron donors, which react irreversibly with the photo-generated holes in VB, can reduce the rapid recombination of photo-generated CB electrons. Organic compounds (hydrocarbons), e.g., methanol, EDTA, ethanol, formaldehyde and lactic acid, are being used widely as electron donors for photocatalytic hydrogen evolution as they can get oxidized by VB holes. The strong reducing electrons left in CB can reduce protons to $H_2$ molecules.

In this project, we will be using the sacrificial agent- $Na_2S/Na_2SO_3$ as ‘hole scavenger’.

Another common solution is to load co-catalysts on the surface of photocatalysts, which can shuttle and store the photogenerated electrons and holes and makes them take part in surface reactions, to produce $H_2$ and $O_2$. $ReO_3$ has been tried to use for such purpose in this project and discussed in chapter 6.

**(2)** An efficient method for separating the simultaneously produced $H_2$ and $O_2$

and suppress their fast backward reaction is yet to be developed. One way is, to combine two photocatalytic reactions on suspended $TiO_2$ powders, using a two-compartment cell furnished with Pt electrodes and a cation-exchange membrane [2]. The back reaction can also be prevented by adding $Na_2CO_3$ salt [3] or Iodide anion. Since overall water splitting is difficult to perform, the photocatalytic activities of a semiconductor for $H_2O$ reduction or oxidation are usually investigated in presence of a sacrificial reagent. Such process is not "overall water splitting", but can be performed as test reactions for the overall water splitting. The basic principle of the same is depicted in Fig. 1.6. When the photocatalysis process is performed in the presence of an electron donor, the photogenerated holes in VB do not oxidize $H_2O$, rather oxidize the electron donor irreversibly, thereby facilitates the reduction of water by CB electrons given that the minimum of the CB of the photocatalyst is positioned above the water reduction potential, Fig. 1.6a. On the other hand, if the reaction is performed in presence of an electron acceptor such as $Ag^+$, instead of reducing $H^+$, electron acceptors get reduced by the photoexcited electrons in CB irreversibly, thus promotes water oxidation by VB holes if the maximum of the VB of the photocatalyst is located below the water oxidation potential, Fig. 1.6b. However, the capability of a semiconductor photocatalyst, to both reduce and oxidize water separately, does not confirm the success of overall water splitting without sacrificial reagents.

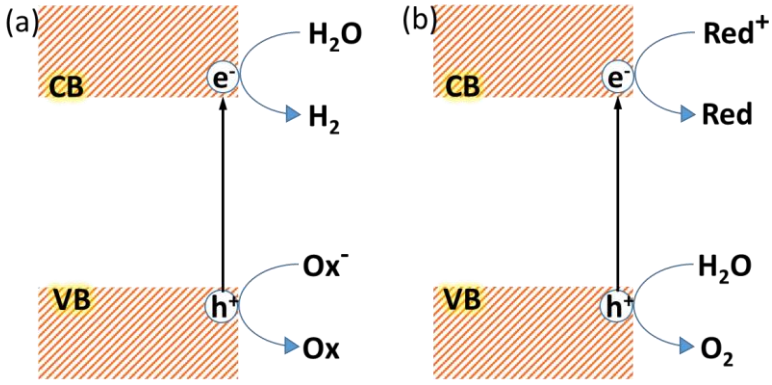


Fig. 1.6. Test reactions for (a) $H_2$ and (b) $O_2$ generation.

**(3)** Although there is an ongoing effort to develop new narrow bandgap visible light active photocatalyst, such as β-$Ge_3N_4$ [4]; chemical modifications of wide band gap materials, to render visible light response, such as, element doping, solid solutions, surface catalyst loading, plasmonic modification and interfacial hetero-junction design have led to significant advancement in the photocatalytic water splitting. This has been discussed in the next chapter in details.

# Chapter 2

## Designing Visible Light active Semiconductor Photocatalyst for Water Splitting

*Photocatalytic water splitting on semiconductors nanoparticles, as practiced in the present dissertation, is a cheap and green way to produce hydrogen fuel. However, at present, the overall efficiency of solar to hydrogen conversion is very low, mainly for some limitations of most common photocatalysts, such as wide bandgap of metal oxide semiconductors and photostability of metal sulfide semiconductors. Although nanostructured semiconductors can help to improve their photocatalytic water splitting efficiency to some limit, nanostructure engineering can not alter their intrinsic electronic properties. Recent advancement in chemical modification of nanostructured semiconductors such as element doping, making solid solutions, surface catalyst loading, plasmonic modification and interfacial hetero-structure design has made inroads into new direction in the photocatalytic water splitting, by enhancing the charge separation, migration, collection and improving the surface reaction kinetics. These strategies that have been adopted in this project, has been discussed in this chapter along with the outline of the thesis.*

## 2.1 Advancements in photocatalytic water splitting

Careful literature review reveals that, research in search of a suitable semiconductor photocatalysts for overall water splitting had largely been devoted to metal oxides, containing metal cations with $d^0$ and $d^{10}$ electronic configurations at the highest oxidation states. The elements, whose metal ions have been found to construct metal oxides active in water splitting is shown in Fig. 2.1.

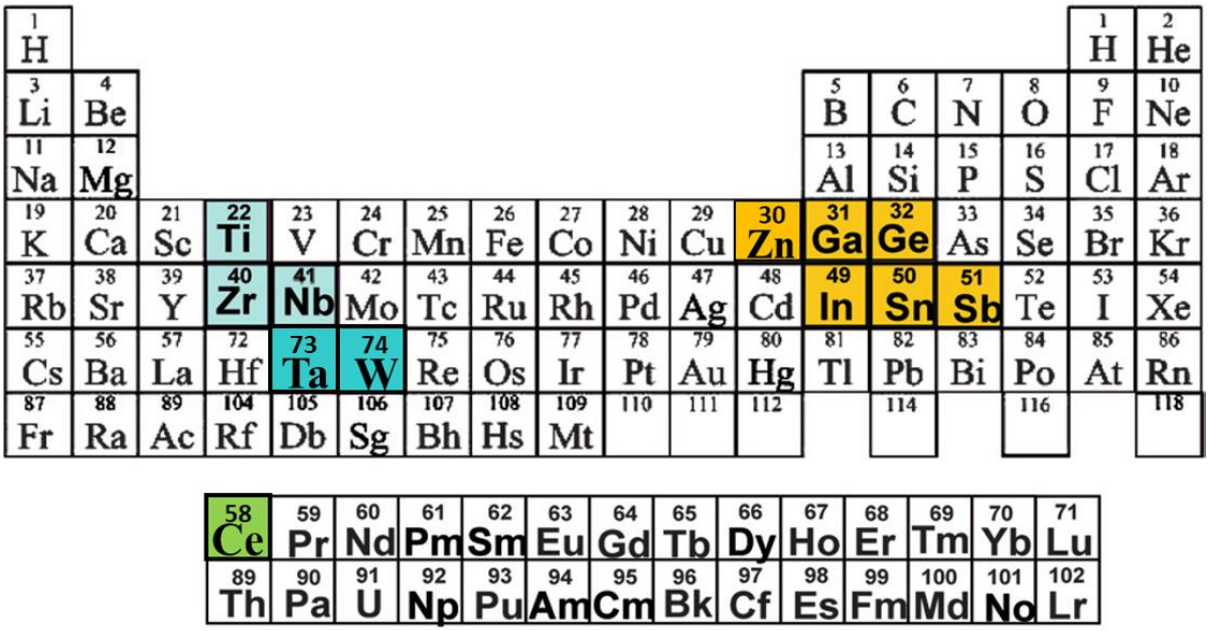


Fig. 2.1. The elements in periodic table used to construct photocatalysts for overall water splitting. Figure adapted from [5].

Three groups of the metal ions have been explored: (1) $d^0$ transition metal ions- $Ti^{4+}$, $Zr^{4+}$, $Nb^{5+}$, $Ta^{5+}$ and $W^{6+}$. (2) $d^{10}$ typical metal ions- $Ga^{3+}$, $In^{3+}$, $Ge^{4+}$, $Sn^{4+}$ and $Sb^{5+}$ and (3) $f^0d^0$ rare earth metal ion- $Ce^{4+}$. Fig. 2.2 shows the some common metal oxides that are used as particulate photocatalyst for water splitting.

## 2.2 Need to utilize visible light

Thus, a group of stable and active photocatalysts for water splitting, comprised solely based on metal oxide systems, such as $TiO_2$, $SrTiO_3$, and ZnO has been examined. However, CB of the metal oxide semiconductor photocatalysts consists of empty orbitals (LUMO) of transition metal cations with $d^0$ and $d^{10}$ configurations or s, p orbitals of typical metals, which is positioned above the water reduction potential (0 V vs NHE

at pH 0) and the level of the VB composed of O2p orbitals is usually ~3.0 eV. Hence the band gap inevitably exceeds 3 eV and the material becomes inactive to use for visible light driven water splitting.

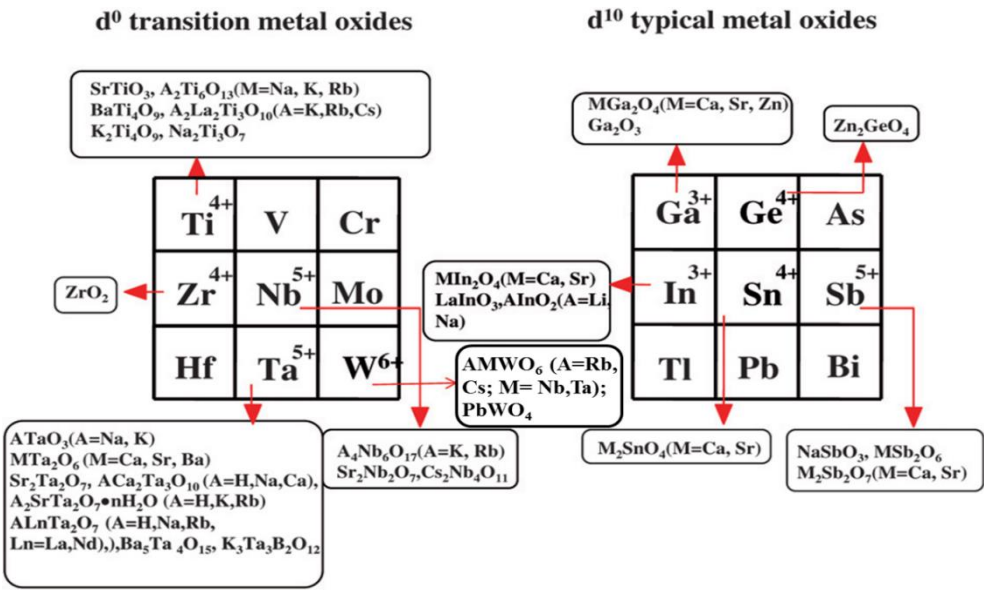


Fig. 2.2. A list of metal oxides with $d^0$ and $d^{10}$ electronic configuration as photocatalysts. Figure adapted from [5].

The band structure potential of typical semiconductors versus normal hydrogen electrode (NHE) potential are shown in Fig. 2.3. Successful and common metal oxide semiconductors with wide band gap, such as $TiO_2$, ZnS and ZnO can cover the water reduction and oxidation potentials, but large bandgap limits their absorption in UV region. For those metal oxides with small bandgap such as $Fe_2O_3$, $BiVO_4$ and $WO_3$, con not generate $H_2$, because their CB edges are too positive than the $H_2$ evolution potential. However, non-oxide materials such as (oxy)nitrides, (oxy)sulphides, and chalgogenides can be potential candidates for water splitting, because, their VB edge shifts negatively, due to their lower electronegativities, and hence N2p and S3p orbitals can form a VB at potentials more negative than that of O2p orbitals, while the potential of the CB remains largely unaffected by N and S. But, visible light active metal sulfides and nitrides are unstable against photocorrosion.

From the above discussion, water splitting by stable metal oxide photocatalysts have been achieved successfully. However, UV light contains only ~3% of the solar energy that reaches the earth, can be utilized for photocatalytic reactions if these are used as catalyst. Visible light comprises ~50% of solar energy. The conversion of solar to $H_2$ efficiency increases with irradiation of longer wavelengths, because the number of photons available in the solar radiation increases in longer wavelength, see Fig. 2.4. Hence, the goal now in photocatalytic water splitting is to effectively employ visible light ($400<\lambda<800$ nm).

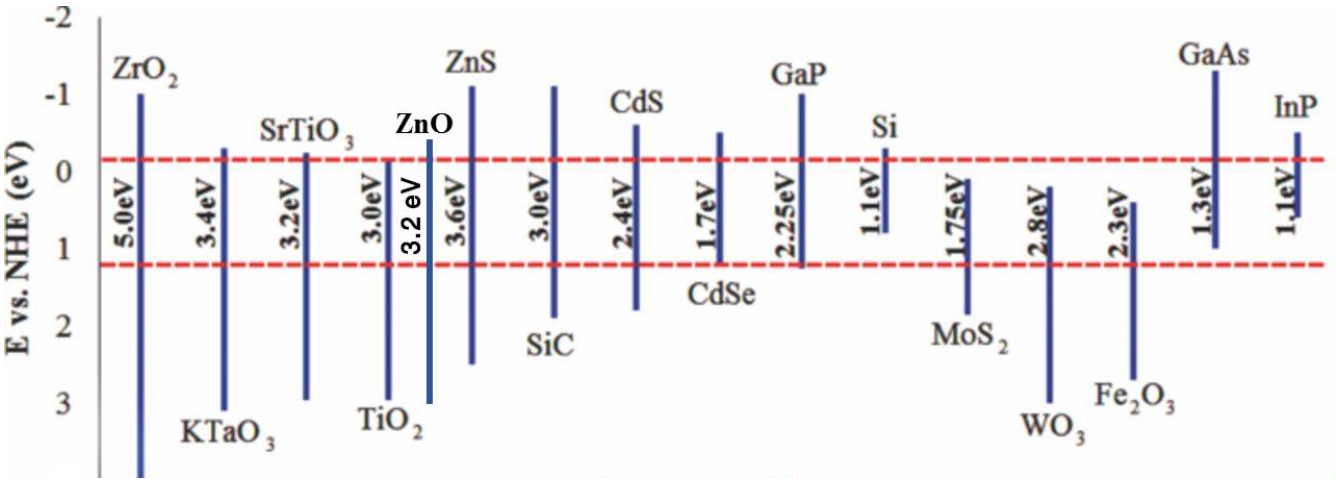


Fig. 2.3. Band positions of semiconductors and redox potentials of water splitting.

## 2.3 Strategies to utilize visible light

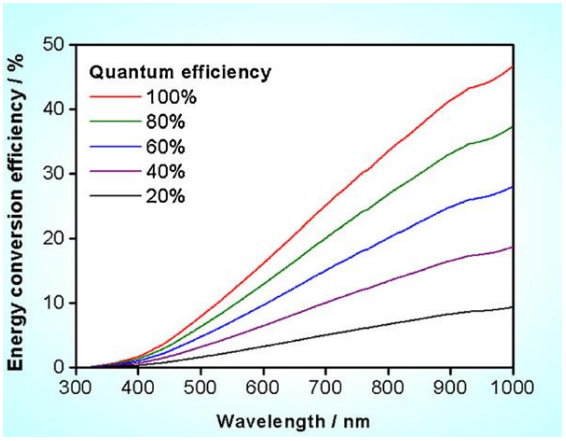


Fig. 2.4. Calculated solar energy conversion efficiency as a function of wavelength. Figure reprinted from [6] with permission. © 2010 American Chemical Society.

The band gap of a visible-light-driven photocatalyst needs to be smaller than 3.0 eV. Therefore, either we need to develop new small band gap photocatalyst, or suitable chemical modification is required to the wide band gap semiconductors to render visible light response. While there is an ongoing effort to develop new narrow bandgap visible light active photocatalyst, such as β-$Ge_3N_4$, $LaTiO_2N$, $Ta_3N_5$ $Sm_2Ti_2S_2O_5$ [6]; band engineering of wide band gap materials, to render visible light response, has led to significant improvement in the photocatalytic water splitting. In this purpose, several strategies were proposed:

(1) Impurity doping.
(2) Preparing visible light responsive solid solution
(3) Designing interfacial hetero-junction.
(4) Plasmonic modification, i.e., loading metallic co-catalyst.
(5) Loading visible light active cocatalyst.

The above mentioned strategies have been considered in the current project and discussed in subsequent chapters.

## 2.4 Band engineering

Suitable band engineering of wide band gap semiconductors can extend the photocatalytic activities under visible light irradiation. For such purpose, a new VB or an electron donor level (DL) need to be created with orbitals of elements other than O2p to make the band gap narrower because the CB level should not be lowered to achieve $H_2$ evolution by reducing water, see Fig. 2.4. Possible strategies can be adopted for the band engineering are shown in Fig. 2.5.

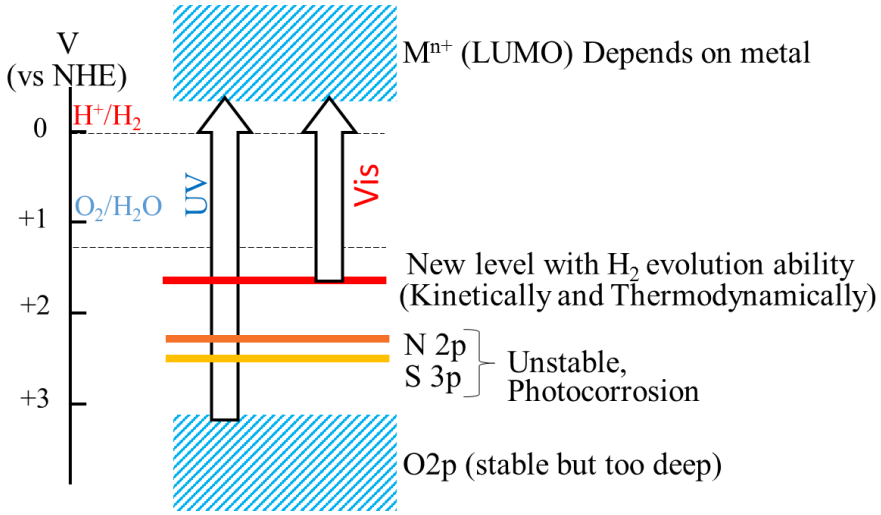


Fig. 2.4. Band control to develop visible light active photocatalyst.

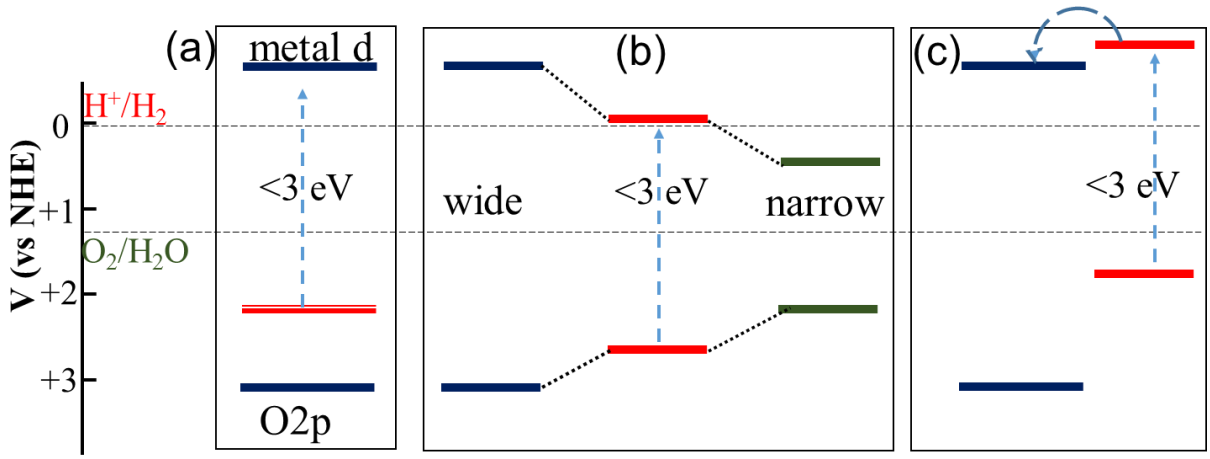


Fig. 2.5. Band engineering strategies to design visible-light driven photocatalysts; (a) doping, (b) solid solutions, and (c) spectral sensitization.

Firstly doping, see Fig 2.5a, the primary doping approaches are follows:

(1) Doping with transition-metal ions that have partially filled d orbital.

(2) VB control using the s orbitals of p-block metal ions or an anion's p orbitals.

If transition-metal cations that has a $d^n$ ($0<n<10$) configuration or anions such as $S^{2-}$, $N^{3-}$, or $C^{4-}$ is doped, a donor or acceptor level will be formed in the forbidden band above the VB consisting of O2p orbitals of the material, lowering down the

Energy gap (for impurity level doping does not create a complete band) as a center for absorption of visible irradiation. Otherwise, Orbitals of Pb 6s in $Pb^{2+}$, Bi 6s in $Bi^{3+}$, Sn 5s in $Sn^{2+}$ and Ag 4d in $Ag^{+}$ can be doped to create new VB above the VB comprised of O 2p orbitals in metal oxide and thus narrows the band gap [7].

But doping frequently affects the photocatalytic activity of a semiconductor, because doping often creates a discreet energy states rather than an energy band and it hinders the rapid diffusion of photoexcited charge carriers. Moreover, maintaining charge balance is difficult if a dopant is introduced, because it creates vacancies in the lattice which act as recombination centers to trap photoexcitons.

Codoping with another suitable dopant can partially address the adverse effects of doping. For example, rutile $TiO_2$ codoped with $Cr^{3+}$ and $Sb^{5+}$ is an effective photocatalyst for water oxidation under visible light [8]. The co-doping also prolongs a lifetime of photogenerated electrons of the $TiO_2$:Cr/Sb photocatalyst. Same has been observed in $SrTiO_3$:$Cr^{3+}$/$Ta^{5+}$, $Cr^{3+}$/$Sb^{5+}$, $Ni^{2+}$/$Ta^{5+}$ and $La_2Ti_2O_7$: Cr/Fe [9]. In this project, codoping in ZnS and CdS has been done and discussed in Chapter 3.

Secondly solid solutions, see Fig. 2.5b, which can also extend the photocatalytic response to the visible range, if a suitable narrow band gap material is chosen to alloy with. We have constructed a series of ZnO:CdO solid solutions and tried to use in visible light driven $H_2$ evolution. This has been discussed in Chapter 4.

Thirdly spectral sensitization, Fig. 2.5c, such as semiconductor nanojunction, semiconductor nano-structures loaded with cocatalysts can be employed to extend the activity to visible range. Here a narrow band gap semiconductor or a cocatalyst acts as antenna to harvest the visible light. ZnO/CdS and $TiO_2$/CdS heterostructures being efficient photocatalysts, a systematic study of their photocatalytic activity depending on the morphology has been carried out in this project and will be discussed in Chapter 5. $ReO_3$ being metallic shows plasmonic absorbance in visible region and tried to use as a cocatalyst, this is discussed in Chapter 6. CuS also absorbs visible light and was used as cocatalyst. This will be discussed in Chapter 7.

# Chapter 3

## Anionic cosubstitution in metal sulfides and application in visible light driven $H_2$ generation[#]

*Anion substitution in inorganic materials, such as metal oxides and sulfides has been a relatively unexplored area in materials chemistry, although it can introduce major changes in the electronic structure and properties. In the current project, P and Cl have been substituted in place of S, in hexagonal CdS and ZnS. The results show that a sub-band of the trivalent anion with strong bonding with the cation appears in the gap just above the valence band, causing a reduction in the band gap significantly. A similar decrease in band gap is observed in N and F cosubstituted in ZnS and CdS. Such anionic substitution helps to improve hydrogen evolution from CdS semiconductor structures and may give rise to other applications as well.*

[#] A manuscript based on this work "*Extraordinary changes in the electronic structure and properties of CdS and ZnS brought about by anionic substitution: Cosubstitution of P and Cl in place of sulfur*" by *Summayya Kouser, S.R. Lingampalli, P. Chitaiah, Anand Roy, Sujoy Saha, Umesh V. Waghmare and C.N.R. Rao* * has been submitted to *Angew. Chem. Int. Ed., 2015*.

## 3.1 Introduction

### 3.1.1 Doping in Nanomaterials

Nanomaterials have been in forefront of science research for past few decades. *"There is plenty of room at the bottom…."* once foreseen by Feynman, is now well-realized by scientific community. Without stopping, endless exploration has opened a new direction in future science and slowly being introduced in everyday life, e.g. LEDs, solar cells, flat panel displays, sensors etc. As the field of semiconductor material continues to evolve towards widespread application, yet there is an immense need of controlling their behaviour precisely for more sophisticated use. Doping gives an additional knob beyond size and shape controlling to extend their capabilities.

### 3.1.2 Need for Research on II-VI Semiconductor

The II-VI semiconductor materials have been studied tremendously due to their wide direct band gap, high extinction co-efficient, high electron-hole mobility etc. Let's talk a bit of some prospects of the II-VI semiconductors, which will help us to address the question, that what is the future scope of this research. II-VI semiconductors have been used extensively. Nevertheless, the application is still in immature age, the drawbacks, in some extent lies in uncertainty of reproducibility, reliability, synthetic techniques and loose grip on their properties. Take the CdTe, having a band gap of 1.5 eV which is believed to be the optimum band gap [10], is considered as the ideal candidate in Photovoltaic Solar Cells (PVSC) and the material cost for PVSCs can be minimized. A considerable efficiency up to 16% has been indeed achieved on CdTe-based PVSC in lab [11], theoretically, which can reach as sky-high of 30% [12]. Take crystalline silicon (c-Si) in other hand, which shares 71% of current PVSC market (2010), has a low extinction coefficient of $\alpha \approx 100\ cm^{-1}$. So a thick layer of ($\gg 1/\alpha$) of Si is needed, and the photoexcitons have to diffuse up to that distance, to contribute to photocurrent [13]. Hence, CdTe can be considered as superior material to c-Si. However, lack of reproducibility and uniformity of CdTe films in large scales has limited it to the best module efficiencies of ~10.7% for CdTe solar cells [13]. Like that, there are immense potentials for II–VI semiconductors in novel applications, but practical utilization still require materials of higher quality with controlled physical and opto-electronic properties. There comes doping into play, to extend the capability.

### 3.1.3 Scope of the Current Project

In this current project we would like to explore the possibility of using two well-known II-VI semiconductors ZnS and CdS for visible light driven photocatalytic water splitting, by modifying with doping. Metal sulfides are interesting candidate for visible light driven photocatalysts. But the stability is a big concern, because of photocorrosion the benefits of band structure is lost, see Eqn 3.1.

$$CdS + 2h^{+} \rightarrow Cd^{2+} + S \qquad (3.1)$$

But, CdS is an excellent photocatalyst for $H_2$ evolution under visible light irradiation if a hole scavenger, such as $S^{2-}/SO_3^{2-}$ exists as mentioned in section 1.3. And, although, it is easy to achieve $H_2O$ splitting with CdS using visible irradiation around 400–450 nm, wider absorption response is still needed. Since there is an activation barrier, a photocatalyst with a 600 nm absorption edge would be optimal.

ZnS, in the other hand, however, possesses a wide band gap, see Fig. 1.3, limiting its application with UV irradiation only. Hence, to make it active under visible irradiation, appropriate doping modification is necessary.

Hence, it is interesting to study if visible-light response can be introduced in CdS and ZnS by doping. In addition, we need to take care of the followings [14]:

(i) The CBM, including subsequent impurity states, should not be lowered down than the $H_2/H_2O$ level to maintain the photoreduction reactivity;

(ii) The states in the gap need to overlap sufficiently with the band states of CdS(ZnS) to facilitate migration of photoexcited carriers to active sites at the surface of the catalyst within their lifetime.

These conditions demand that we dope anionic species rather than cationic metals, which often give quite localized d states deep in the band gap and result in recombination centers of carriers or an acceptor level below the CBM can be created, disturbing condition i. Calculations by Asahi et al. for densities of states (DOSs) of the substitutional doping of C, N, F, P, or S for O in $TiO_2$, show desired band-gap narrowing, fulfilling the above conditions as well [14]. Hence, we would like to use anionic species as dopant, but to address some adverse effects of doping, as discussed earlier, we will follow co-doping strategy.

Recently, our lab has introduced co-substitution of anion in materials. Tremendous change in material properties have been seen by co-substituting O with N and F, in ZnO [15] and $TiO_2$ [16]. Both ZnO and $TiO_2$ have attractive properties like its abundance, nontoxicity, band structure, high chemical and photostabilities,. A limitation, however, is that these semiconductor materials only absorb in UV region. Co-doping served the purpose as a means to extend the absorption into the visible and showed enhanced hydrogen evolution on interaction with visible light.

We want to employ similar concept in CdS and ZnS. This kind of co-substitution chemistry has been a relatively unexplored area, although very interesting chemistry is underlying there. Based on the works above, we see that the p orbitals of N are effective to create a mid-gap band near to the VB, effectively reducing the band gap, whereas the presence of F enhances the incorporation of N into the lattice. Because oxides and nitride–fluorides have similar structural preferences, the co-substitution $2O^{2-} \rightarrow N^{3-} + F^{-}$ preserves the cation to anion ratio and does not change the average anion radius significantly, and such co-substitution would not create O vacancies. Same time, the strong electron-withdrawing ability of F increases the surface acidity and photoinduced hydrophilicity, which makes the recombination of photoexcitons hard, preparing the material to act as a better photocatalyst. Hence, it is important to explore the effect of co-substitution in CdS and ZnS as well.

For the opto-electronic applications of II–VI nanomaterials, it is essential to do desired amount of doping in order to achieve bipolar electrical conduction and increased carrier concentration, i.e. efficient p- and n- type doping, is needed. Nevertheless, research on doping, of II–VI nanomaterials is yet to reach a suitable and reliable stage. In table 3.1, I have tried to summarize the present status of the research of doping into II-VI nanostructure by various techniques.

Table 3.1: research status on doping of II–VI nanostructures.

| | n- type doping | | | | | p- type doping | | | | | Transition metal | | | | | | | |
|---|---|---|---|---|---|---|---|---|---|---|---|---|---|---|---|---|---|---|
| | Al | Ga | In | F | Cl | N | P | As | Sb | Ag | Cu | Mg | Mn | Zn | Fe | Co | Ni | Cr |
| CdS | [17] | [18] | [19] | [20] | [21] | [22] | [23] | [24] | [25] | [26] | [27] | [28] | [29] | [30] | [31] | [32] | [33] | [34] |
| ZnS | [35] | [36] | [37] | [38] | [39] | [40] | [41] | | [25] | [42] | [42] | [43] | [44] | | [45] | [46] | [47] | [48] |

While a number of intriguing results has been provided by the studies, but they also arouses a number of questions unaddressed. In particular, there are serious concern about the existence of anion doping and co-doping. If anion co-doped materials can be prepared, what is the dependence between photocatalytic activities and composition, and how to control the relation? The percentage of the dopants in the previous studies are low. We think that it is important to prepare co-doped nanomaterials with fairly high amount dopants and study their properties. The earlier discussion also suggests that it would be attractive to pursue same strategy to co-substitute with P and Cl. For this purpose four works were tried:

1: P, Cl co-substitution in CdS

2: P, Cl co-substitution in ZnS

3: N, F co-substitution in CdS

4: N, F co-substitution in ZnS.

Various semiconductor materials have been employed in photocatalytic water splitting, $TiO_2$ has been celebrated most among them owing to its low-cost, nontoxicity, and stability. However, ZnS and CdS nanoparticles bear tremendous potential to act as a better photocatalyst. ZnS is widely studied for its relatively high reactivity for $H_2$ evolution, even without loading noble metal cocatalysts [49]. The theoretical efficiency of photocarrier generation in ZnS, as a direct band gap semiconductor, is much more than that of $TiO_2$. Actually, some ZnS photocatalyst exhibit superior photocatalytic efficiencies than $TiO_2$ [50]. ZnS is supposed to be one of the effective photocatalysts, because of its rapid generation of photoexcitons and the highly negative redox potentials of photoexcited electrons; however its photocatalytic performance of ZnS is restricted due to its wide band gap. Moreover, the photocatalytic activity of ZnS is seriously hindered by the fast recombination of photoexcitons. CdS, on the other hand, is suitable for visible light response; however, it is prone to photocorrosion in the long-term photocatalytic reactions. Therefore, the photocatalytic performance of ZnS and CdS still needs to be revised. Non-metal ion co-doped photocatalysts have showed immense promise, owing to that it can improve photocatalytic activity by extending the spectral response to visible light region and supressing the recombination of photogenerated charge carriers. Hence, we expect that anion co-substituted CdS and ZnS will exhibit better photocatalytic activity.

## 3.2 Experimental Section

### 3.2.1 Preparation of CdS(ZnS) nanoparticles

In a typical preparation, 30 mmol of cadmium acetate dihydrate (or zinc acetate dihydrate) was dissolved in 50 ml water. To this, 40 mL solution of 30 mmol sodium sulphide ($Na_2S$) was added dropwise with vigorous stirring. The stirring was continued 10 mins further. The resultant precipitate (CdS or ZnS) was centrifuged, washed with water and acetone and air dried in 70 °C oven, then ground and stored for future use.

### 3.2.2 Preparation of CdS(ZnS):P,Cl

Cd powder (3 mmol) and red phosphorus (2.5 mmol) were ground uniformly and made as a pellet. The sample was heated at 450 °C for 2h in nitrogen flow in a tube furnace. The resulting product (cadmium phosphide, $Cd_3P_2$) was ground uniformly and used for further studies. CdS nanoparticles (2 mmol), $Cd_3P_2$ (0.1 mmol) and $NH_4Cl$ (0.6 mmol) were ground uniformly and made as a pellet. The pellet was heated at 400 °C for 6h in nitrogen atmosphere in a tube furnace and cooled naturally. In a second method, CdS nanoparticles (2 mmol), red phosphorus (2 mmol) and $NH_4Cl$ (1 mmol) were ground uniformly and made as a pellet. The pellet was heated at 350 °C for 2h in nitrogen atmosphere in a tube furnace and cooled naturally. The resulting sample was ground uniformly and again made as a pellet. This sample was heated at 400 °C for 1h in nitrogen atmosphere and cooled naturally to obtain CdS:P,Cl.

To prepare ZnS:P,Cl; Zn powder (3 mmol) and P (2.5 mmol) were ground uniformly and made as a pellet. The pellet was heated at 350 °C for 2h followed by heating at 400 °C for 2h in nitrogen atmosphere in a tube furnace. After the reaction, the resulting product (zinc phosphide, $Zn_3P_2$) was ground uniformly and used for further studies. ZnS (3 mmol), $Zn_3P_2$ (0.15 mmol) and $NH_4Cl$ (0.9 mmol) were uniformly ground and made as a pellet. The pellet was heated at 600 °C for 6h in nitrogen atmosphere in a tube furnace and cooled naturally. The resulting sample ($CdS_{1-x-y}P_xCl_y$ or $ZnS_{1-x-y}P_xCl_y$) was ground uniformly and used for further characterization.

### 3.2.3 Preparation of CdS(ZnS):N,F

CdS(ZnS) (3 mmol) and $NH_4F$ (40 mmol) were uniformly ground and transferred

to a ceramic boat and placed in a tube furnace. The sample was heated at 600 °C for 2h in a continuous flow of ammonia. After the reaction the temperature was allowed to cool down to room temperature naturally. The resulting product ($CdS_{1-x-y}N_xF_y$, or $ZnS_{1-x-y}N_xF_y$) was ground uniformly and characterized.

## 3.3 Results and Discussion

### 3.3.1 Characterizations

P, Cl cosubstituted CdS was synthesized successfully starting from cubic CdS nanoparticles, see experimental section for preparation. The PXRD patterns of the starting material and product are shown in Fig. 3.1a. The XRD patterns confirms the presence of hexagonal CdS:P,Cl in the product. Hence, phase transformation of cubic CdS to wurtzite CdS is seen, which is expected, because of the strain in the lattice caused by the cosubstitution of P, Cl in place of S.

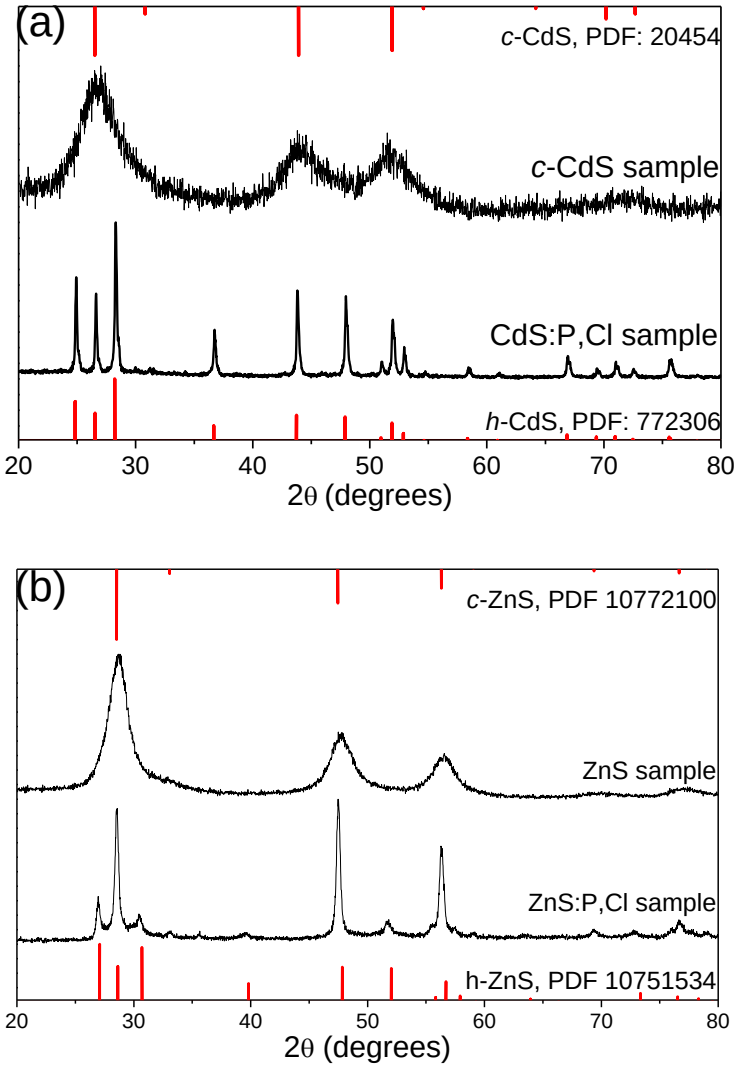


Fig. 3.1. PXRD patterns of undoped and P,Cl cosubstituted (a) CdS, and (b) ZnS.

The Absorption spectra of the CdS:P,Cl is shown in Fig. 3.2a. For comparison, the absorption of hexagonal CdS is also shown. The absorption edge of the doped sample has extended further in the visible region, as predicted in the introduction, the band gap is shown in inset. Color of the sample also changed to brownish from orange.

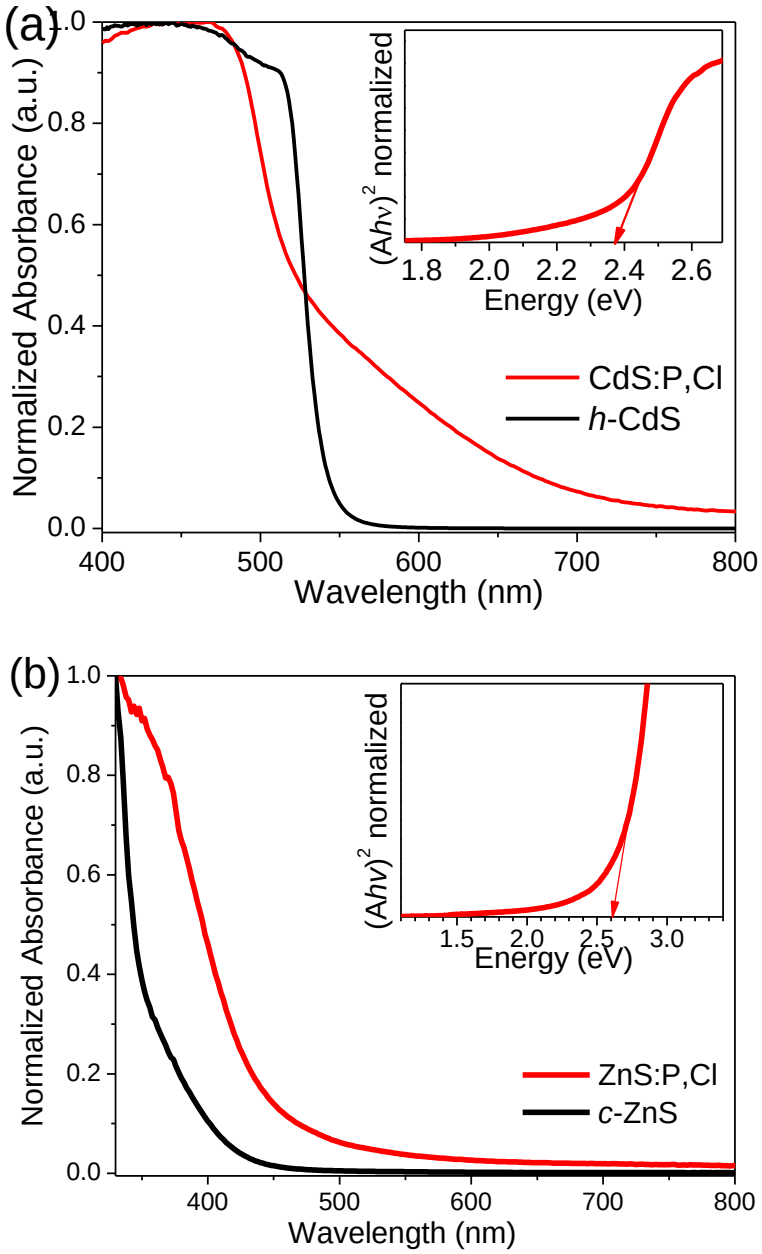


Fig. 3.2. UV-vis spectra of P,Cl codoped (a) CdS, and (b) ZnS samples. Inset shows the Tauc plot.

The band gap was obtained by Tauc Plotting. The energy of the optical band gap can be obtained by using the following equation:

$$\alpha h\vartheta = B\left(h\vartheta - E_g\right)^m$$

Where, $E_g$ is the band gap and B is a constant. Here, considering the direct band gap nature of CdS, the value of m has to be taken ½. Here absorption coefficient α, is proportional to the absorbance A, given the sample concentration and path length constant, and hence can be replaced with A. The absorption values was obtained from solid state diffuse reflectance values following KM function. Inset figure shows the plot of $(Ah\nu)^2$ vs $h\nu$ for the sample. The band gap is obtained by extrapolating the linear part of the curves to the intercept on X axis.

Presence of the P and Cl in the doped CdS(ZnS) samples are confirmed by XPS and shown in Fig. 3.3. The composition of the sample obtained $CdS_{0.7}P_{0.14}Cl_{0.15}$.

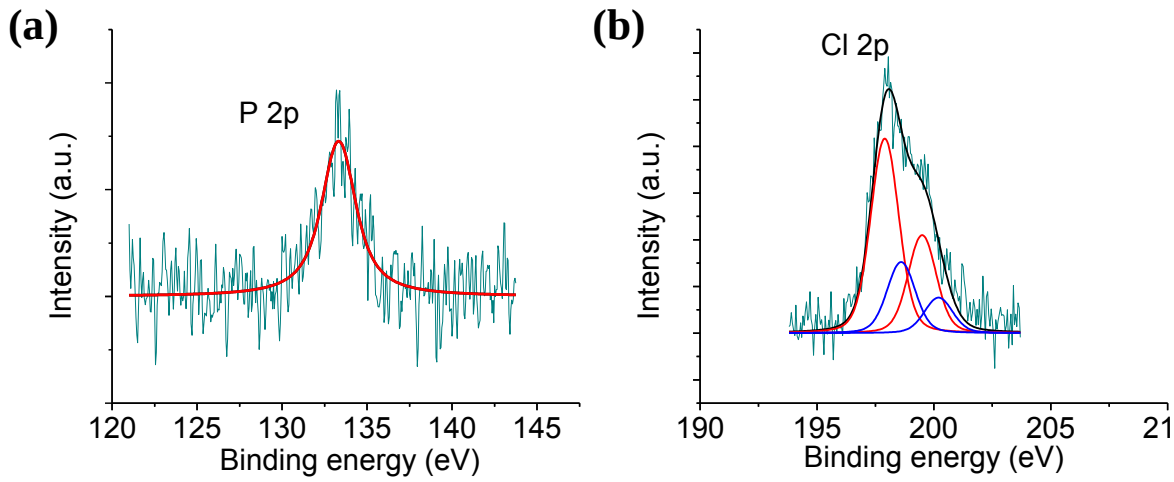


Fig. 3.3. High resolution XPS of (a) P 2p and (b) Cl 2p in CdS:P,Cl.

Similarly, ZnS:P,Cl was synthesized successfully starting from cubic ZnS nanoparticles, which is confirmed by PXRD patterns, see Fig. 3.1b. The absorption of the doped ZnS is also extended to the visible region, see Fig. 3.2. Band gap also decreased to 2.6 eV, compared to 3.9 eV bandgap of hexagonal ZnS. The presence of P and Cl is confirmed by XPS and the composition found to be $ZnS_{0.8}P_{0.1}Cl_{0.1}$.

To examine the morphology of the doped nanoparticles TEM image was obtained and shown in Fig. 3.4, which shows spherical nanoparticles of 100-500 nm.

N, F cosubstituted CdS(ZnS) was prepared starting from cubic CdS(ZnS). The UV-vis spectra of the ZnS:N,F sample is shown in Fig. 3.5. Here also extension of absorption towards longer wavelength is seen. Accordingly the bandgap decreased, 2.6 eV, which is reflected in the pale red color of the doped sample. PXRD pattern confirms presence of *c*-ZnS in the product, see Fig. 3.6.

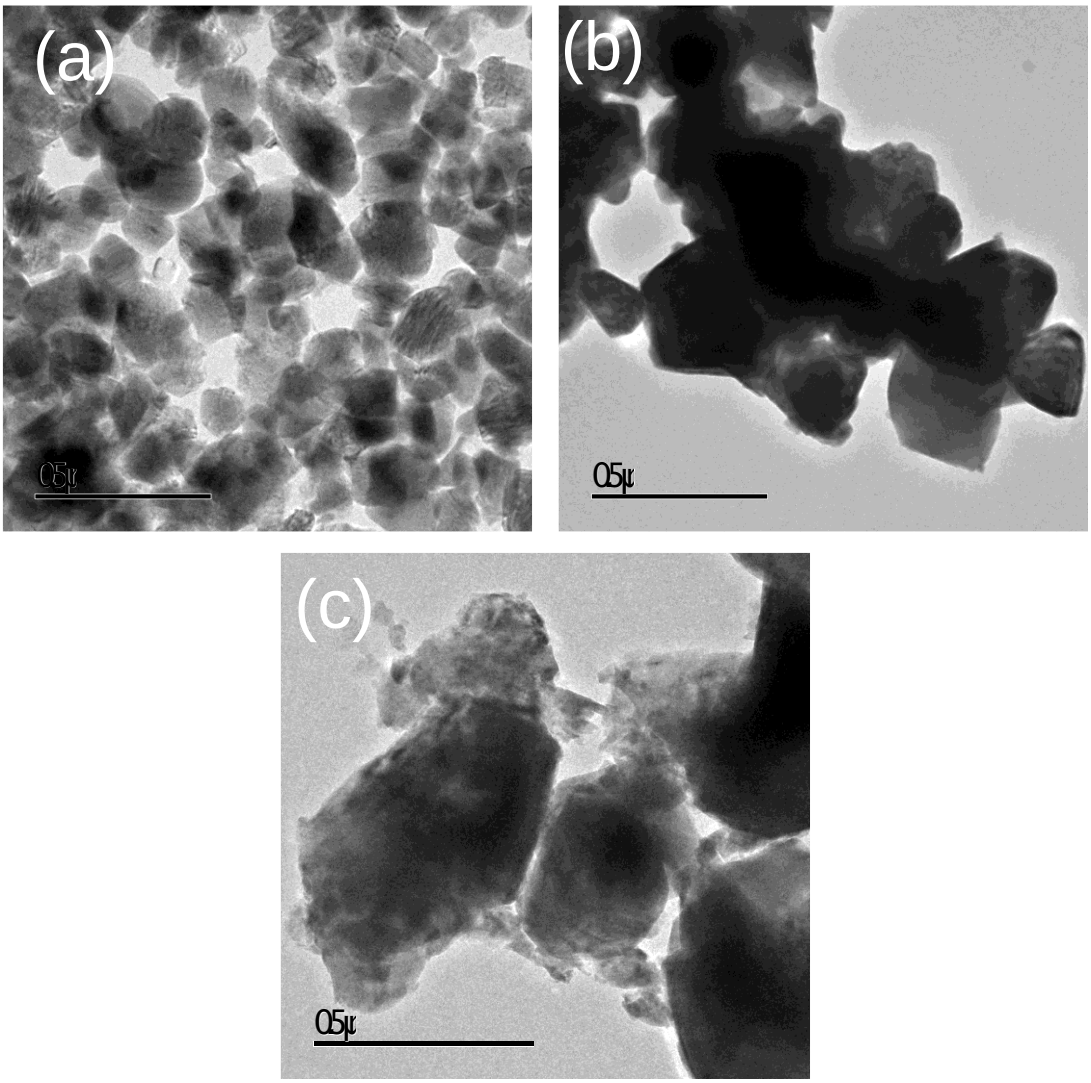


Fig. 3.4. TEM image of (a) ZnS:P,Cl (b) CdS:P,Cl and (c) ZnS:N,F samples.

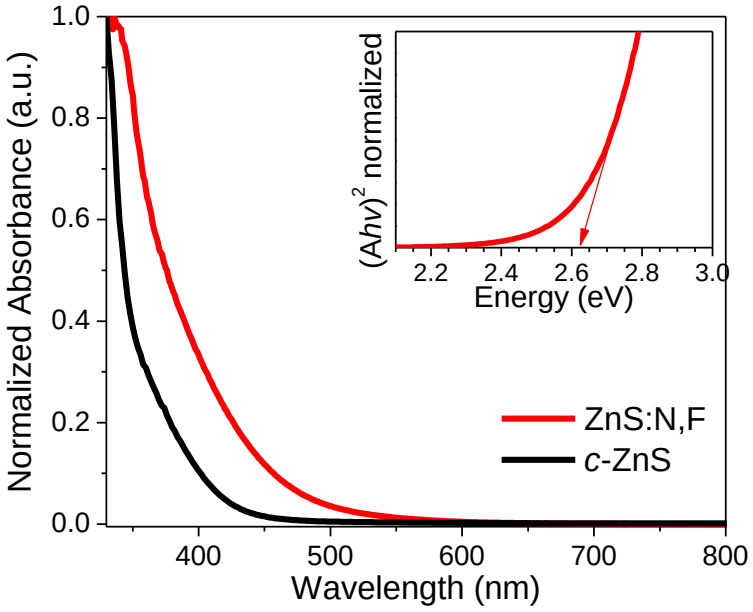


Fig. 3.5. Absorption Spectra of ZnS:N,F. Inset shows the band gap.

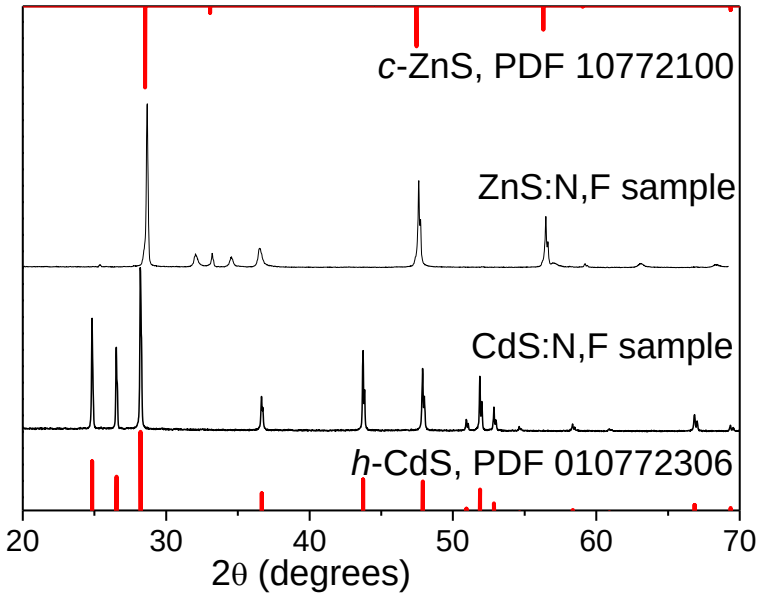


Fig. 3.6. PXRD pattern of doped CdS and ZnS samples.

Absorption spectra of CdS:N,F sample prepared is shown in Fig. 3.7. PXRD pattern confirms *h*-CdS in the product, see Fig. 3.6. The presence of N and F in the doped ZnS sample was confirmed by XPS. The composition of the product has found to be $ZnS_{0.7}N_{0.15}F_{0.17}$. The XPS of CdS:N,F sample is yet to be done.

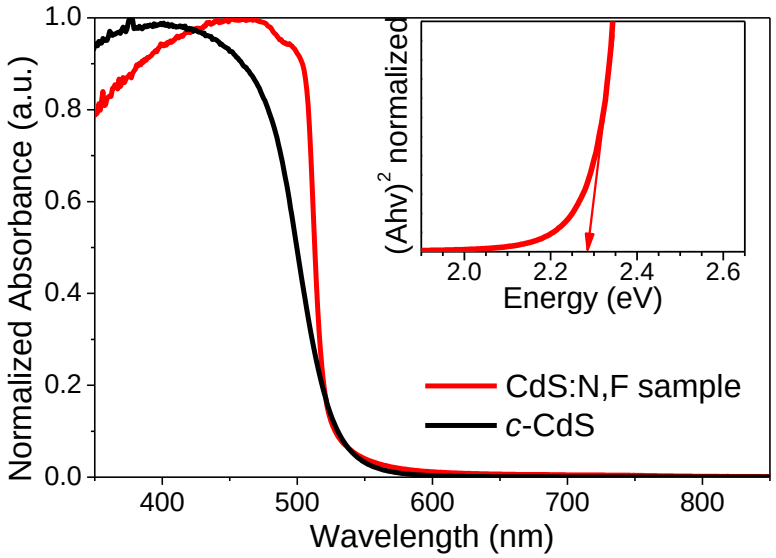


Fig. 3.7. Absorption spectra of CdS:N,F sample

### 3.3.2 Photocatalytic Activity

The above samples were employed in visible light drive photocatalytic water splitting to study $H_2$ evolution efficiency. The CdS:P,Cl, sample, prepared by the

second method, showed superior photocatalytic activity than undoped CdS and the result is shown in Fig. 3.8.

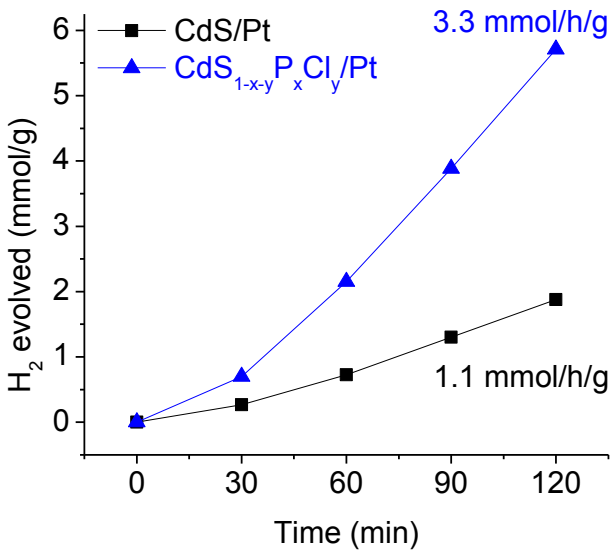


Fig. 3.8. Visible-light induced $H_2$ evolution by CdS/Pt and $CdS_{1-x-y}P_xCl_y$/Pt

The other samples did not show any improvement in activity. The reason for this is lots of recombination pathway created for doping, which can be expected for doped samples. However, further optimization in preparation condition and dopant concentration is needed to obtain defect free crystal structure, and that will surely render better photocatalytic activity.

## 3.4 Conclusion

In conclusion, anion cosubstitution in ZnS and CdS has brought significant change in material properties. P,Cl and N,F cosubstitution in place of S in the above mentioned metal sulfides has reduced the band gap as expected. The absorption of ZnS(CdS) has been extended towards longer wavelength, which leads to visible light response. Thus ZnS(CdS) could be used in visible light driven water splitting. Cosubstituted CdS has exhibited better $H_2$ evolution efficiency than undoped CdS. Hence, doping could be considered as an efficient band engineering strategy to render visible light activity in wide band gap photocatalyst.

# Chapter 4

## Synthesis of $Zn_{1-x}Cd_xO$ solid solution and Visible light driven water splitting by the ZnCdO/CdS heterostructures

*Rendering visible light activity in a wide band gap semiconductor, by making solid solution with a small band gap semiconductor, is being practiced recently. Similar strategy has been adopted to ZnO, which is a well-known wide band gap semiconductor and active in UV irradiation. For this purpose CdO is thought to help, since it can absorb visible light. Hence a series of $Zn_{1-x}Cd_xO$ solid solutions have been prepared and water splitting by $Zn_{1-x}Cd_xO$/CdS heterostructures has been carried out and discussed in this chapter. But this heterostructure did not show desired efficiency in hydrogen generation.*

# 4.1 Introduction

To devise a new photocatalyst which can split water under visible irradiation, the semiconductor solid solution has drawn considerable interest. Preparing a solid solution is a useful band engineering method, as discussed in chapter 2. Certain wide band gap photocatalysts become visible light active through solid solution formation with appropriate modification with $H_2$ evolution cocatalysts and stability of the photocatalyst has found to be increased. Such as, solid solutions of GaN and ZnO ($(Ga_{1-x}Zn_x)(N_{1-x}O_x)$) and $ZnGeN_2$ and ZnO ($(Zn_{1+x}Ge)(N_2O_x)$), $AgInS_2$-$CuInS_2$ are capable of overall water splitting after loading suitable $H_2$ evolution cocatalysts [51].

In this project, we would like to study the visible light driven hydrogen generation by $Zn_{1-x}Cd_xO$ solid solution. ZnO having a band gap of 3.2 eV, only absorbs in UV region, but it is an excellent photocatalyst owe to its stability. Hence, to make it visible light responsive, alloying with CdO with band gap 2.2 eV, has been tried. ZnCdO solid solution has the advantage of tunability of band gap, allowing control over the absorption in larger spectrum from near UV to visible. However, preparing the solid solutions is difficult, because of alloying materials with different crystalline structures, ZnO is hexagonal whereas CdO is cubic. Herein, $Zn_{1-x}Cd_xO$ solid solution with x= 0, 0.2, 0.4, 0.6, 0.8, 1 has been prepared and characterised. For visible light driven water splitting $Zn_{1-x}Cd_xO$/CdS heterostructures was prepared and employed for hydrogen generation.

# 4.2 Experimental Section

## 4.2.1 Synthesis of $Zn_{1-x}Cd_xO$

In a typical synthesis 4(1-x) mmol zinc acetate dihydrate and 4x mmol of cadmium acetate dihydrate was dissolved in 60 mL water (x= 0, 0.2, 0.4, 0.6, 0.8, 1). To this solution, 10 mL of hydrogen peroxide was added dropwise while stirring. After 20 mins, 10 mL solution of 8 mmol KOH was added dropwise and stirring was continued for further 20 mins. The resulting white precipitate was centrifuged and washed with water and acetone and air dried in 70 $^oC$ oven. The product was collected and ground and the calcined at 250 $^oC$ in air for 2 h followed by natural cooling. The calcined sample is the desired product and grounded nicely to use for next step.

### 4.2.2 Synthesis of $Zn_{1-x}Cd_xO$/CdS heterostructure

To prepare 20 mol% CdS loaded ZnCdO, 100 mg of $Zn_{1-x}Cd_xO$ was dispersed in 40 mL water. To this, 10 mL solution containing desired amount of cadmium acetate dihydrate and another 10 mL solution containing desired amount of $Na_2S$ was added dropwise simultaneously with stirring. The contents were kept stirring further 20 mins. The resulting precipitate was centrifuged and washed with water and acetone and air dried in 70 $^oC$ oven. The product was collected and ground to use for water splitting.

## 4.3 Results and Discussion

### 4.3.1 Characterization of ZnCdO solid solutions

The $Zn_{1-x}Cd_xO$ solid solutions were prepared successfully with x= 0, 0.2, 0.4, 0.6, 0.8, 1. Fig. 4.1 shows the absorption spectra of the samples. We can see that ZnO absorption edge is 400 nm, and absorption gradually extends towards visible range with forming solid solution with CdO, uptil 700 nm for highest amount of CdO.

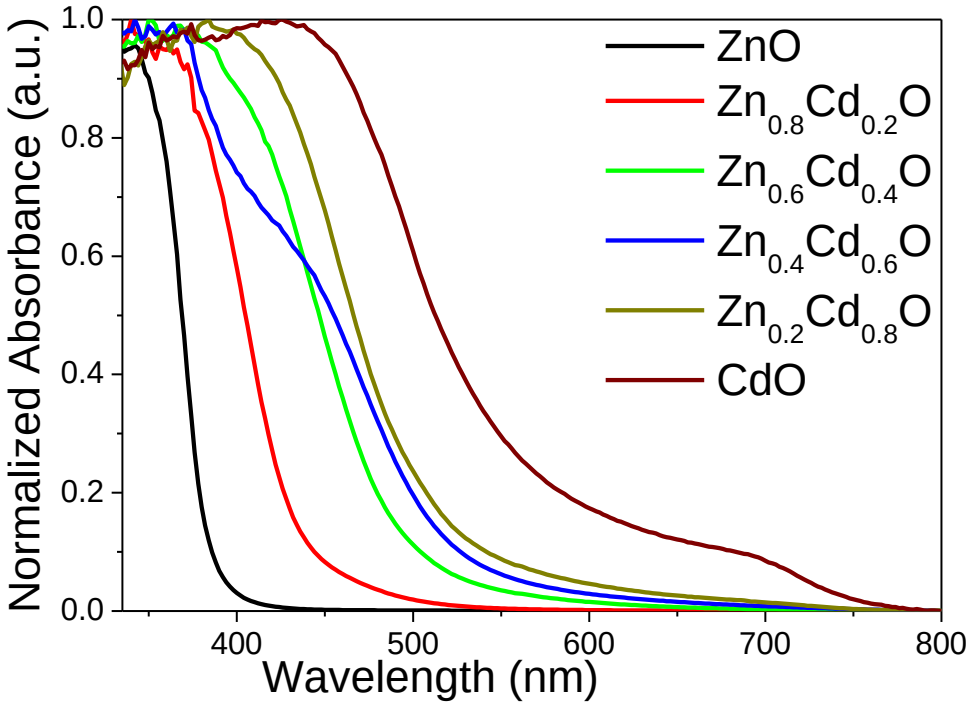


Fig. 4.1. Absorption spectra of $Zn_{1-x}Cd_xO$ samples.

Gradual decrease in band gaps is also clear from the Tauc plot, Fig. 4.2a. ZnO (x= 0) shows band gap of 3.3 eV, whereas bandgaps of 2.9, 2.6, 2.56, 2.5 and 2.3 eV

are seen in case of x= 0.2, 0.4, 0.6, 0.8 and 1, respectively. The color of the sample also seen to change gradually, see Fig. 4.2b. Thus the ZnCdO solid solutions allow the tunability and utilization of entire visible spectrum.

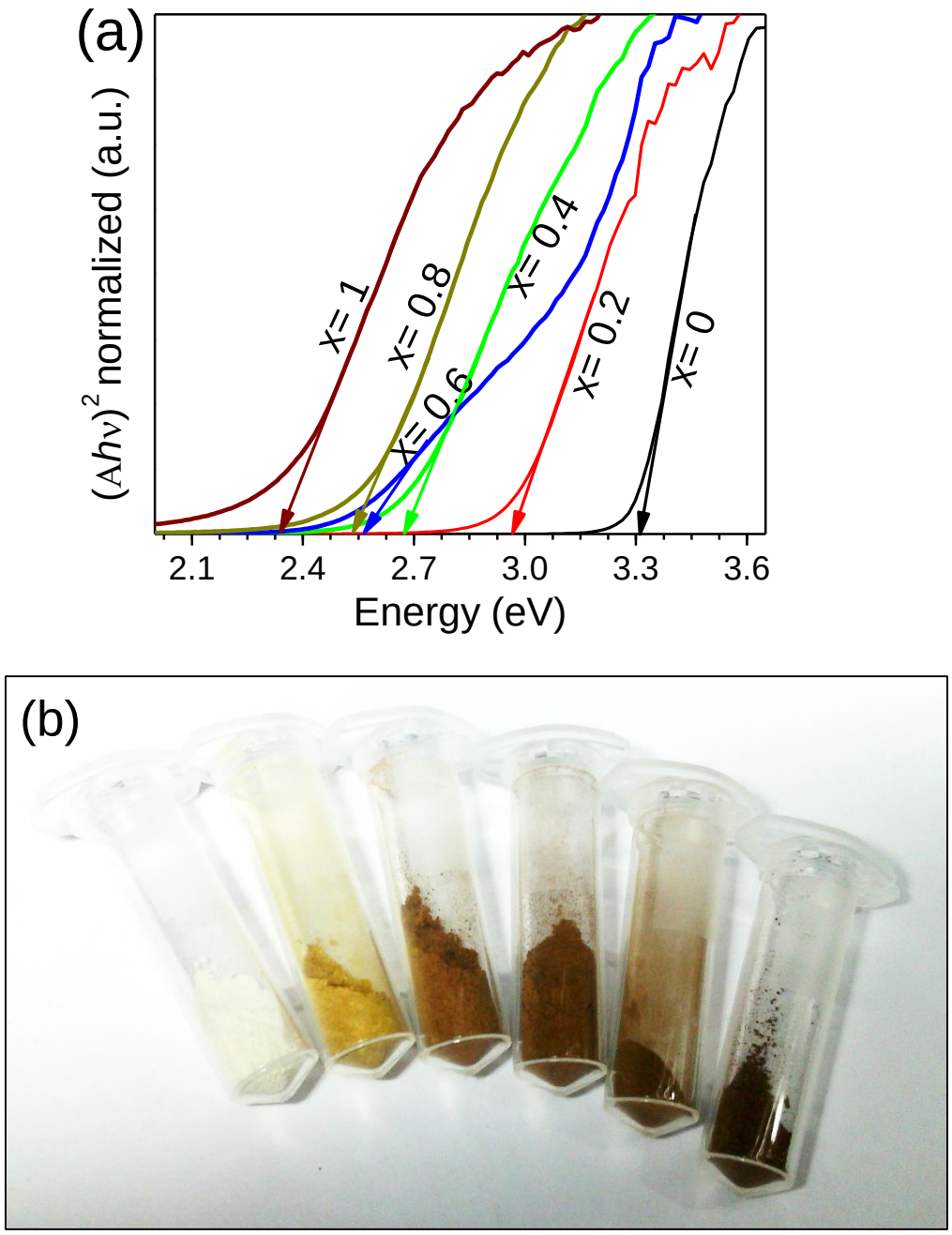


Fig. 4.2. (a) Tauc Plot of $Zn_{1-x}Cd_xO$ samples, (b) Color of the $Zn_{1-x}Cd_xO$ samples, from left x= 0, 0.2, 0.4, 0.6, 0.8, 1.

XRD pattern of the $Zn_{1-x}Cd_xO$ samples prepared are shown in Fig. 4.3. The patterns confirms the presence of ZnO/CdS solid solution with desired concentration.

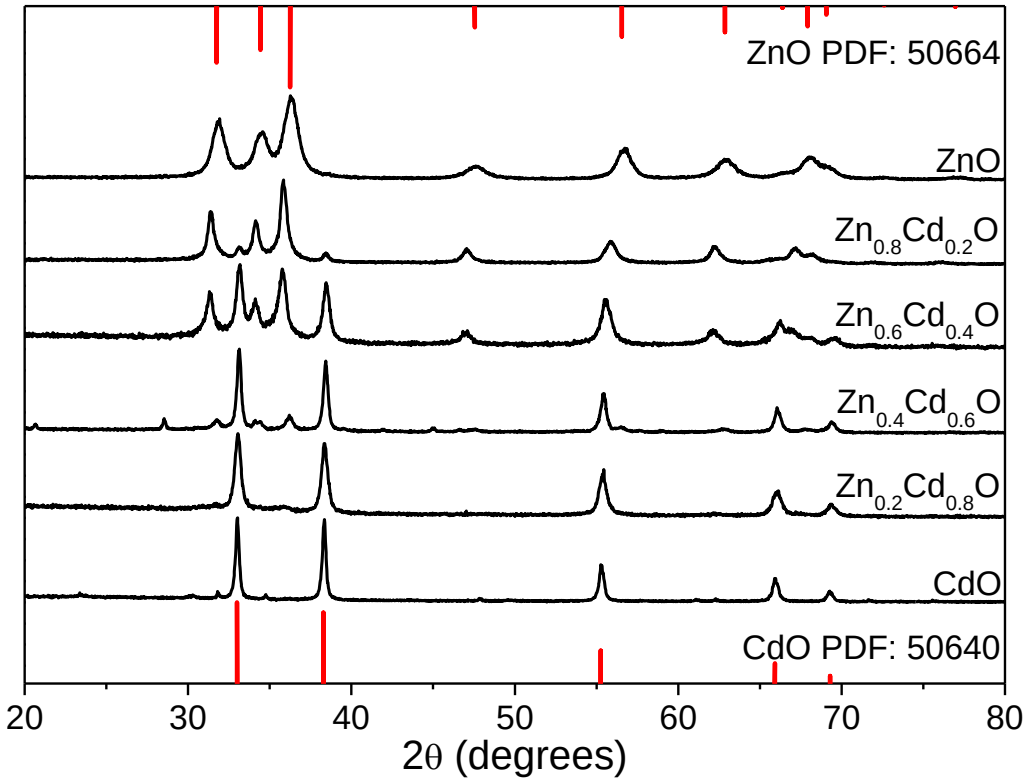


Fig. 4.3. XRD pattern of $Zn_{1-x}Cd_xO$ samples.

### 4.3.2 Photocatalytic activity of ZnCdO

To explore the water splitting efficiency, 20 mol% of CdS cocatalyst was deposited to $Zn_{1-x}Cd_xO$ solid solutions for x= 0.2, 0.4, 0.6. Fig. 4.4 shows the absorption spectra of the $Zn_{1-x}Cd_xO/CdS^{20\%}$ heterostructures. It is evident that the loading of CdS cocatalyst further extends the absorption of $Zn_{1-x}Cd_xO$ solid solution

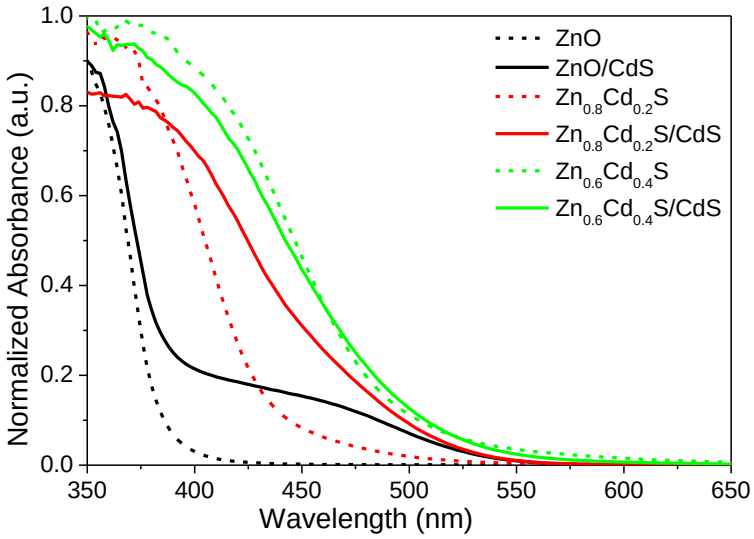


Fig. 4.4. Absorption spectra of the $Zn_{1-x}Cd_xO/CdS^{20\%}$ heterostructures

towards visible spectrum. These heterostructure was subjected photocatalytic activity investigation to by measuring $H_2$ evolution in visible light in the presence of $Na_2S$ and $Na_2SO_3$ as sacrificial agents. The results is shown in Fig. 4.5a.

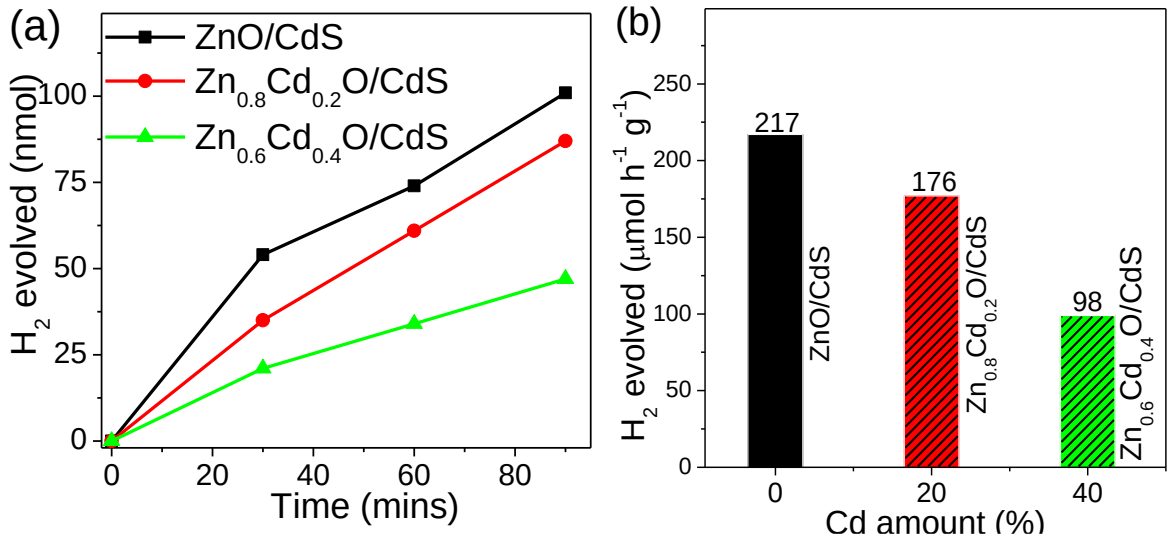


Fig. 4.5. Photocatalytic $H_2$ evolution by $Zn_{1-x}Cd_xO/CdS^{20\%}$ heterostructures.

The ZnO/CdS is found to be most active in photocatalytic $H_2$ evolution, and the activity decreases with increasing amount of CdO. The photocatalytic $H_2$ evolution rate is highest in the case ZnO/CdS (217 μmol $h^{-1}g^{-1}$) and least in the case of $Zn_{0.6}Cd_{0.4}O/CdS$ (98 μmol $h^{-1}g^{-1}$), see Fig. 4.5b. In spite of having broader absorption in visible range in case of ZnCdO solid solution we observe less photocatalytic activity.

## 4.4 Conclusion

A series of metal oxide solid solutions $Zn_{1-x}Cd_xO$ were synthesized successfully and characterized by XRD and UV–visible absorption spectra. The photocatalytic properties of the $Zn_{1-x}Cd_xO$ solid solutions were investigated. However, the $Zn_{1-x}Cd_xO/CdS$ solid solution did not show improvement in photocatalytic efficiency, rather the visible light induced $H_2$ evolution rate decreased with increased amount of CdO in the solid solution, despite better absorption property in visible region. The low efficiency achieved by the solid solutions can be due to inefficient charge transfer which need to be investigated. However, the activity of this solid solution may be expected to be effective by refining the synthesis process.

# Chapter 5

## Morphology dependent visible light induced hydrogen generation on $ZnO(TiO_2)/CdZnS$ and $ZnO(TiO_2)/Pt/CdZnS$ heterostructures[#]

*Effects of morphology and surface area on photocatalytic hydrogen generation have been studied by using the $ZnO(TiO_2)/Cd_{1-x}Zn_xS$ and $ZnO(TiO_2)/Pt/Cd_{1-x}Zn_xS$ ($x$=0, 0.2) heterostructures with different nanostructures of ZnO and $TiO_2$. In the case of $TiO_2/Pt/Cd_{0.8}Zn_{0.2}S$ heterostructures highest $H_2$ evolution rates up to 1.76 mmol $h^{-1}g^{-1}$ were obtained with $H_2Ti_3O_7$ nanotubes, with the least $H_2$ evolution rates (0.55 mmol $h^{-1}g^{-1}$) from $TiO_2$ powder (Degussa P-25). In the case of ZnO/Pt/CdS heterostructures the highest $H_2$ evolution rate (6.88 mmol $h^{-1}g^{-1}$) was obtained from ZnO nanorods1, whereas the least $H_2$ evolution rate (2.55 mmol $h^{-1}g^{-1}$) was obtained from ZnO nanorods3. The photocatalytic activity of the heterostructures generally follows the trend in BET surface areas of the oxide nanostructures, with high surface area favoring great hydrogen evolution activity. Defects such as oxygen vacancies seem to decrease hydrogen evolution.*

[#] A manuscript based on this work "*Effects of morphology and surface area of the oxide nanostructures on the visible light induced generation of hydrogen in $ZnO(TiO_2)/Cd_{1-x}Zn_xS$ and $ZnO(TiO_2)/Pt/Cd_{1-x}Zn_xS$ heterostructures ($x$= 0.0, 0.2).*" by *Anand Roy, S. R. Lingampalli, Sujoy Saha and C. N. R. Rao** has been submitted to *Chem Phys Lett., 2015*.

## 5.1 Introduction

Aiming the utilization of solar energy, where research was initially triggered by the $TiO_2$-based photoelectrochemical reactions for the splitting of water into $H_2$ and $O_2$, a considerable number of materials have been studied as powder photocatalysts. This lists a group of transition metal oxides composed of metal ions with $d^0$ and $d^{10}$ electronic configuration. Thus, a bunch of successful photocatalysts has been found for water splitting, comprised mainly based on metal oxide systems. Although, some non-oxide materials have been examined, for example, CdS and CdSe, especially for visible light induced photocatalysis, successful semiconductor photocatalytic systems are yet to achieve, primarily for the inability to use visible solar spectrum, inefficient charge separation and migration and inherent deleterious degradation side reactions leading towards instability of the materials.

### 5.1.1 Solid State Z-Scheme

Water splitting with some single photocatalysts has been performed successfully, such as $TiO_2$ and ZnO as discussed in earlier. However, the absorption edge of the common active photocatalysts are mostly lies in UV region. Z-scheme water splitting enables an advantage over one-step photoexcitation water splitting, because visible light of a wider range can be employed. When two or more suitable semiconductor systems are combined, mimicking Z-scheme, the photogenerated electrons from the semiconductor with a higher CBM can diffuse to the other with a lower CBM, and this can occur even without the reversible redox shuttles, because of the interparticle electron transfer via the interfacial physical contact between the photocatalysts. Single photocatalysts can be doped or alloyed, as discussed previously, but that offers less flexibility to change the electronic structure and low separation efficiency of photoexcitons for recombination pathways, the hybrid or integrated multi-semiconductor systems are expected to give significant advantages by facilitating the separation of electron–hole pairs more and also makes the reduction and oxidation process to happen at two different photocatalysts.

### 5.1.2 Why Heterostructures

An efficient photocatalyst are comprised of of two basic components: a light

absorbing antenna and a redox catalyst. To design an efficient photocatalyst, some requirements must be followed. Firstly, the semiconductor light absorbing site should possess a band gap large enough to generate energetic electrons ($E_g \gg 1.23$ eV, practically >2.0 eV). Also, the band gap of the semiconductor should be a smaller enough to have effective absorption overlap with the solar visible spectrum ($E_g \ll 3.0$ eV). Second, a mechanism to drive charge separation and migration process efficiently should be there. Furthermore, the semiconductor light absorbing site have to be in close integration with the redox catalysts to facilitate effective utilization of the photoexcited carriers for the desired photochemical reactions. Lastly, the photoelectrochemical stability of the system to be maintained. Since a single semiconductor system can hardly fulfil all the requirements, whereas heterostructures can ensure these, facilitating the three step of photocatalytic water splitting, by:

(1) Enhance photon absorption; for instance, a narrow band gap semiconductor or molecules having a large absorption coefficient can be employed to sensitize the semiconductor materials with wide band gaps.
(2) A p–n junction (semiconductor/semiconductor) or a Schottky junction (metal/semiconductor) can be created to facilitate direct and effective charge separation and migration without recombination.
(3) Cocatalyst effect: combining with proper cocatalyst creates more active site and lowers the redox overpotential at those active sites.

### 5.1.3 Morphology and Surface area

While designing a stable and efficient photocatalytic system for water splitting, the architecture and the surface properties of the heterogeneous photocatalyst have to be considered rigorously. Nanosized semiconductor particles greatly enhance the photocatalytic activity, and moreover, nanostructure diversity like nanoparticles, nanotubes, porous nanospheres, nanowires, nanorods and other structures have exhibited unconventional properties, and can further offer new degrees of freedom in selection of the material and designing an effective photocatalytic system. For instance, nanostructured photocatalyst with more surface area can create more active sites for the desired surface redox reactions. Size dependent property, like, quantum confinement effect in nanostructured semiconductors and surface plasmonic absorption property in metallic cocatalyst, renders new direction for engineering the

solar energy absorption processes. Also, the diverse nanostructures can enrich the flexibility to integrate multiple functional sites to create interfacial heterostructures with desired characteristics and efficiency. For example, $Cr_2O_3$ shell can supress the back reaction of $H_2$ to form $H_2O$ on noble metal cocatalyst [6]. Hence careful tailoring of both the surface and volume properties of the semiconductor heterostructure needs to be considered to obtain high photoactivity in water splitting.

### 5.1.4 Scope of Present Study

In this study, we have explored morphology-dependent photocatalytic hydrogen evolution on $ZnO(TiO_2)/Cd_{1-x}Zn_xS$ and $ZnO(TiO_2)/Pt/Cd_{1-x}Zn_xS$ (x=0.0, 0.2) haterostructures containing different nanostructures of ZnO and $TiO_2$. This work has been motivated by recent studies on ZnO/CdS [52] and $CdS/TiO_2$ [53] haterostructures for $H_2$ evolution under visible light irradiation. Good $H_2$ evolution properties of ZnO/Pt/CdS and $ZnO/Pt/Cd_{1-x}Zn_xS$ configuration, have also been observed in our lab previously [54]. Photochemical activity of such semiconductor materials would be expected to depend on the morphology and surface area. For example, $TiO_2$ nanofibres are reported to exhibit superior photocatalytic activity than $TiO_2$ nanoparticles [55]. Morphology-dependent photocatalytic activities of ZnO nanostructures have also been noted [56]. Hence we considered to carry out a systematic study of the dependence of visible-light induced hydrogen generation by semiconductor haterostructures containing oxide nanostructures. We have prepared ZnO and $TiO_2$ nanostructures with different morphologies and surface areas and investigated visible-light induced hydrogen generation by $TiO_2/Cd_{0.8}Zn_{0.2}S$, ZnO/CdS, $TiO_2/Pt/Cd_{0.8}Zn_{0.2}S$ and ZnO/Pt/CdS heterostructures.

## 5.2 Experimental section

Different $TiO_2$ and ZnO nanostructures, prepared by someone else, were employed to prepare the heterostructures. Nanoparticles of $Cd_{0.8}Zn_{0.2}S$ (20 mol%) were deposited $TiO_2$ by adding methanolic solution of $Cd(CH_3COO)_2$, $2H_2O$ (0.02 M, 10 mL)and $Na_2S$ (0.04 M, 10 mL) dropwise in the presence of $Zn(CH_3COO)_2$, $2H_2O$ (4.5 mM, 8 mL) to a methanolic dispersion of $TiO_2$ nanostructures. To prepare the

$TiO_2$/Pt/$Cd_{0.8}Zn_{0.2}S$ heterostructures, first Pt nanoparticles were deposited on the surface of $TiO_2$ nanostructures. To do so, $TiO_2$ (1 mmol) was dispersed in distilled water under sonication, to which chloroplatinic acid (0.5 mol %) and methanol (15 mL) were added and kept in UV light (New Port 6279, Xe-Lamp 400W) for 1.5 hours. The brownish black colored $TiO_2$/Pt product was collected and washed, centrifuged with methanol. Then $Cd_{0.8}Zn_{0.2}S$ (20 mol%) nanoparticles were deposited on $TiO_2$/Pt by the drop wise addition of $Cd(CH_3COO)_2$, $2H_2O$ (0.02 M, 10 mL), and $Na_2S$ (0.04 M, 10 mL) in methanolic solution. A solution of $Zn(CH_3COO)_2$, $2H_2O$ (4.5 mM, 8 mL) was added prior to adding $Cd^{2+}$ and $S^{2-}$ to form $Cd_{0.8}Zn_{0.2}S$ nanoparticles. ZnO/Pt/CdS heterostructures were also synthesized similarly. ZnO (1 mmol) was dispersed in distilled water, to which chloroplatinic acid (0.5 mol %) and methanol (15 mL) were added. The mixture was sonicated and $NaBH_4$ (0.82 mmol) solution was added drop wise to this dispersion in order to reduce chloroplatinic acid in to Pt. The brownish product was washed with methanol and centrifuged. Nanoparticles of CdS (20 mol %) were deposited on the ZnO/Pt heterostructures by drop-wise addition of a methanolic solution of $Cd(CH_3COO)_2$, $2H_2O$ (0.02 M, 10 mL) and $Na_2S$ (0.04 M, 10 mL).

## 5.3 Results and Discussion

### 5.3.1 $TiO_2$ Nanostructures

In the case of $TiO_2$ based heterostructures, we have used (a) $TiO_2$ nanopowder (Degussa P25) (b) $TiO_2$ NPs (c) $H_2Ti_3O_7$ NT and (d) $TiO_2$ NT. The diameter of Degussa P25 and the synthesized $TiO_2$ NPs, $H_2Ti_3O_7$ NTs and $TiO_2$ NTs were in the ranges 20-30, and 7- 14 nm, 6-12 and 5-8 nm respectively. The surface areas of Degussa P25, $TiO_2$ NPs, $TiO_2$ NTs, and $H_2Ti_3O_7$ NTs were 39.9, 123, 247.85, and 248.69 $m^2/g$ respectively by BET surface area measurements.

### 5.3.2 Photocatalytic activity of $TiO_2$ Heterostructures

We carried out photocatalytic study, by measuring $H_2$ evolution with visible light irradiation in the presence of $Na_2S$ and $Na_2SO_3$ as sacrificial agents. Since partial substitution of Zn in CdS is known to increase the photocatalytic activity [54], we therefore synthesized the $TiO_2$/$Cd_{0.8}Zn_{0.2}S$ as well as $TiO_2$/Pt/$Cd_{0.8}Zn_{0.2}S$

heterostructures by employing the four $TiO_2$ nanostructures. Fig. 5.1a shows a typical low magnification TEM image of $TiO_2$NT/Pt/$Cd_{0.8}Zn_{0.2}S$ heterostructures. The Pt and $Cd_{0.8}Zn_{0.2}S$ nanoparticles can be seen on the surface of the $TiO_2$ nanotubes.

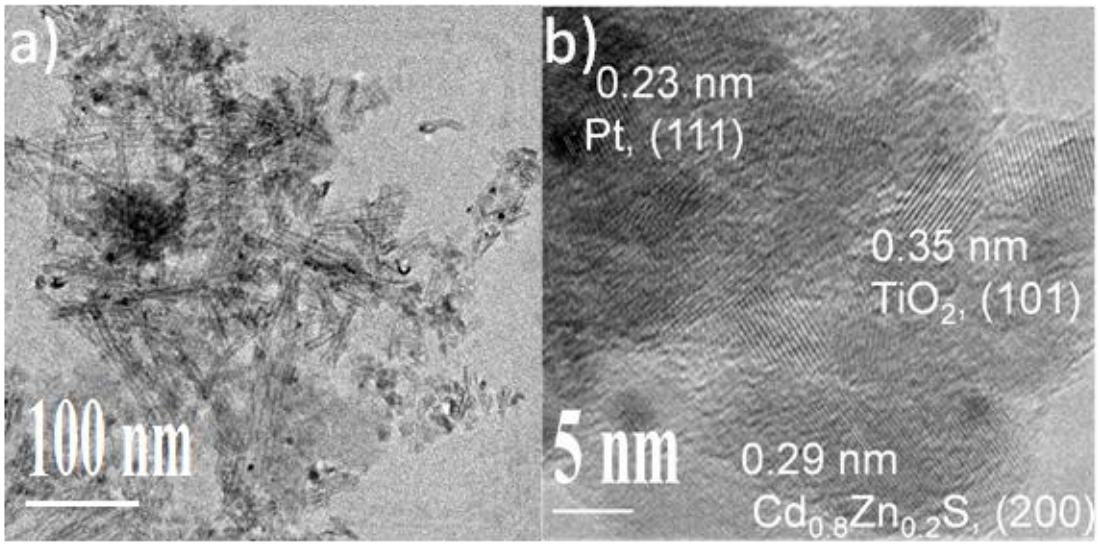


Fig. 5.1. (a) TEM image (b) HRTEM image of $TiO_2$ NT/Pt/$Cd_{0.8}Zn_{0.2}S$ heterostructures.

A HRTEM image of this heterostructures further shows the lattice spacing of 0.35 nm of $TiO_2$, 0.29 nm of $Cd_{0.8}Zn_{0.2}S$ and 0.23 nm of Pt corresponding to the 101 plane of $TiO_2$, 200 plane of $Cd_{0.8}Zn_{0.2}S$ and 111 plane of Pt (Fig. 5.1b).

Photocatalytic $H_2$ evolution activities of $TiO_2$/$Cd_{0.8}Zn_{0.2}S$ heterostructures with the different $TiO_2$ nanostructures are shown in Fig. 5.2a. The photocatalytic $H_2$ evolution rate is highest in the case $H_2Ti_3O_7$ nanotubes (104 μmol $h^{-1}g^{-1}$) and least in the case of $TiO_2$ nanoparticles (18 μmol $h^{-1}g^{-1}$). The photocatalytic activity of $TiO_2$ NTs (93 μmol $h^{-1}g^{-1}$) is close to that of the $H_2Ti_3O_7$ nanotubes. In spite of having higher surface area we observe less photocatalytic activity of synthesized $TiO_2$ nanoparticles than $TiO_2$ powder (Degussa P25) (36 μmol $h^{-1}g^{-1}$), probably due to the presence of unremoved capping agents. We have also explored the photocatalytic activity of $TiO_2$/Pt/$Cd_{0.8}Zn_{0.2}S$ heterostructures with the different $TiO_2$ nanostructures, see Fig. 5.2b. In the presence of Pt nanoparticles we see a significant increase in the photocatalytic activity of all the heterostructures. The highest photocatalytic $H_2$ evolution is from the heterostructures formed with $H_2Ti_3O_7$ nanotubes (1.76 mmol $h^{-1}g^{-1}$) and least from the $TiO_2$ powder (Degussa P25) nanoparticles (0.55 mmol $h^{-1}g^{-1}$).

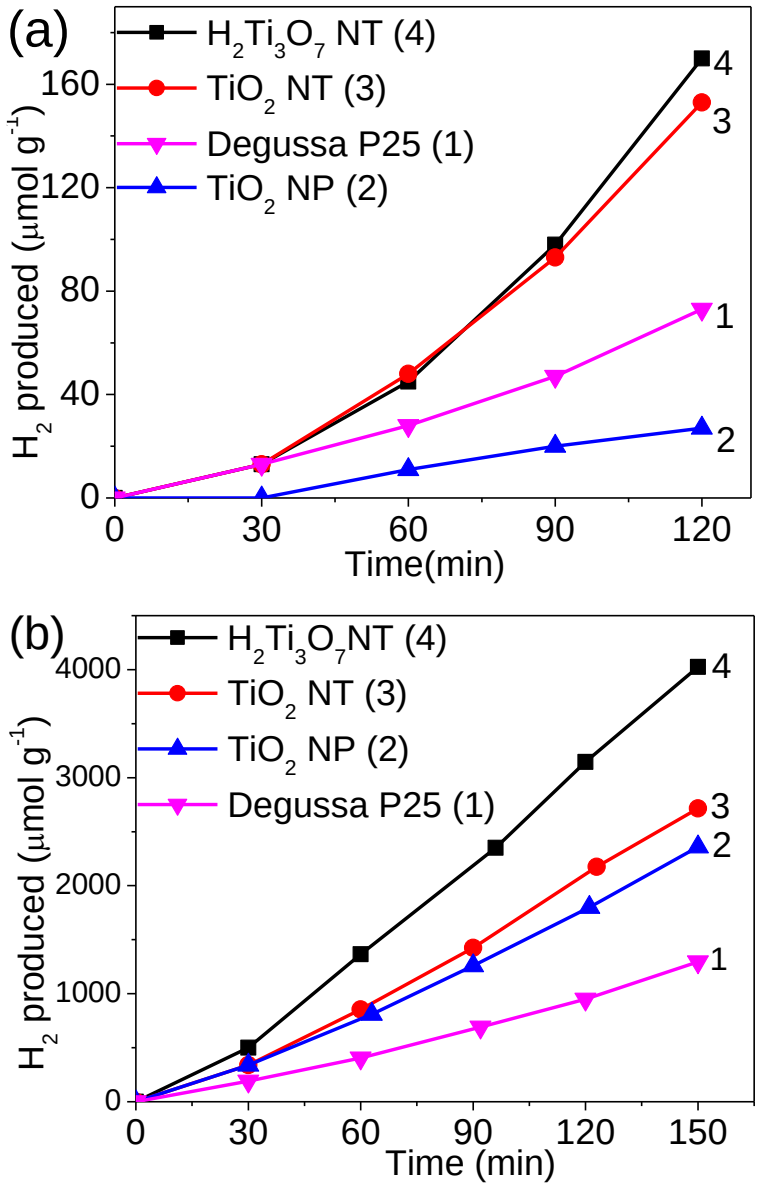


Fig. 5.2. Photocatalytic activity of (a) $TiO_2/Cd_{0.8}Zn_{0.2}S$, (b) $TiO_2/Pt/Cd_{0.8}Zn_{0.2}S$ heterostructures employing different $TiO_2$ nanostructures.

The photocatalytic $H_2$ evolution follows the trend of the surface areas of the different $TiO_2$ nanostructures (Fig. 5.3). We clearly see that the $H_2Ti_3O_7$ nanotubes with highest surface area show highest photocatalytic activity whereas Degussa P25 with the lowest surface area shows the least activity.

### 5.3.2 ZnO Nanostructures

We have studied the effect of morphology of the various ZnO nanostructures on the photochemical $H_2$ evolution by the ZnO/CdS and ZnO/Pt/CdS heterostructures

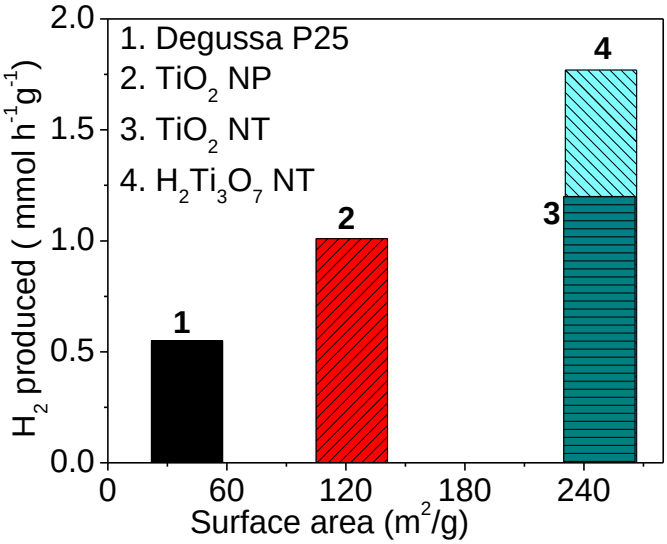


Fig. 5.3. Photocatalytic $H_2$ evolution from $TiO_2$/Pt/$Cd_{0.8}Zn_{0.2}S$.

by employing the following nanostructures of ZnO. (a) ZnO NP, (b) ZnO NR1, (c) ZnO NR2 and (d) ZnO NR3 as NR1 but with greater length and diameter. The ZnO nanoparticles had the diameter in the 10-20 nm range; ZnO NR1 had rods of 30-50 nm lengths, and 12-20 nm diameter. ZnO NR2 had the lengths in the range 100-300 nm and diameters in the 20-35 nm range. ZnO NR3 had lengths in the range 600-800 nm and diameters in the 50-110 nm range. BET Surface areas of ZnO NPs, ZnO NR1, ZnO NR2, and ZnO NR3, are 45.3, 41, 17.6, 8.7 $m^2/g$ respectively.

Fig. 5.4a shows the TEM image of ZnONR2/Pt/CdS heterostructures. The nano particles of Pt and CdS can be seen on the surface of ZnO nanorods. A HRTEM image

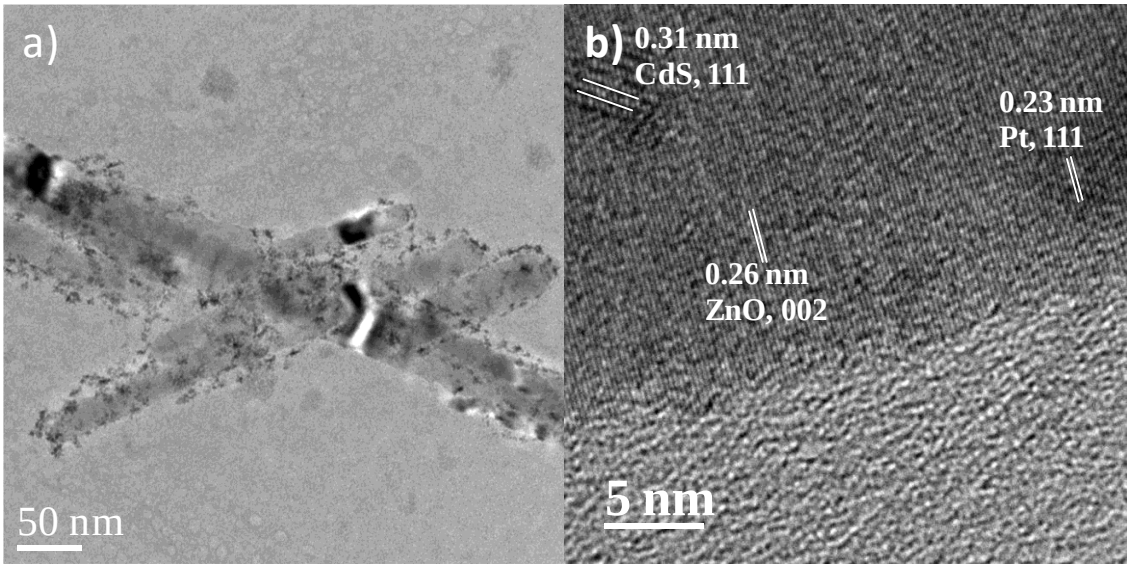


Fig. 5.4. (a) TEM image; (b) HRTEM image of ZnO NR2/Pt/CdS.

of the heterostructure (Fig. 5.4b) further shows lattice spacing of 0.26, 0.31, and 0.23 nm corresponding to 002 plane of ZnO, 111 plane of CdS and 111 plane of Pt.

### 5.3.4 Photocatalytic Activity of ZnO Heterostructures

Photocatalytic $H_2$ evolution from ZnO/CdS and ZnO/Pt/CdS heterostructures were studied under visible light irradiation in the presence of $Na_2S/Na_2SO_3$ sacrificial agent. Fig. 5.5a shows the photocatalytic activity of the ZnO/CdS heterostructures with different ZnO nanostructures. The photocatalytic $H_2$ evolution activity from the

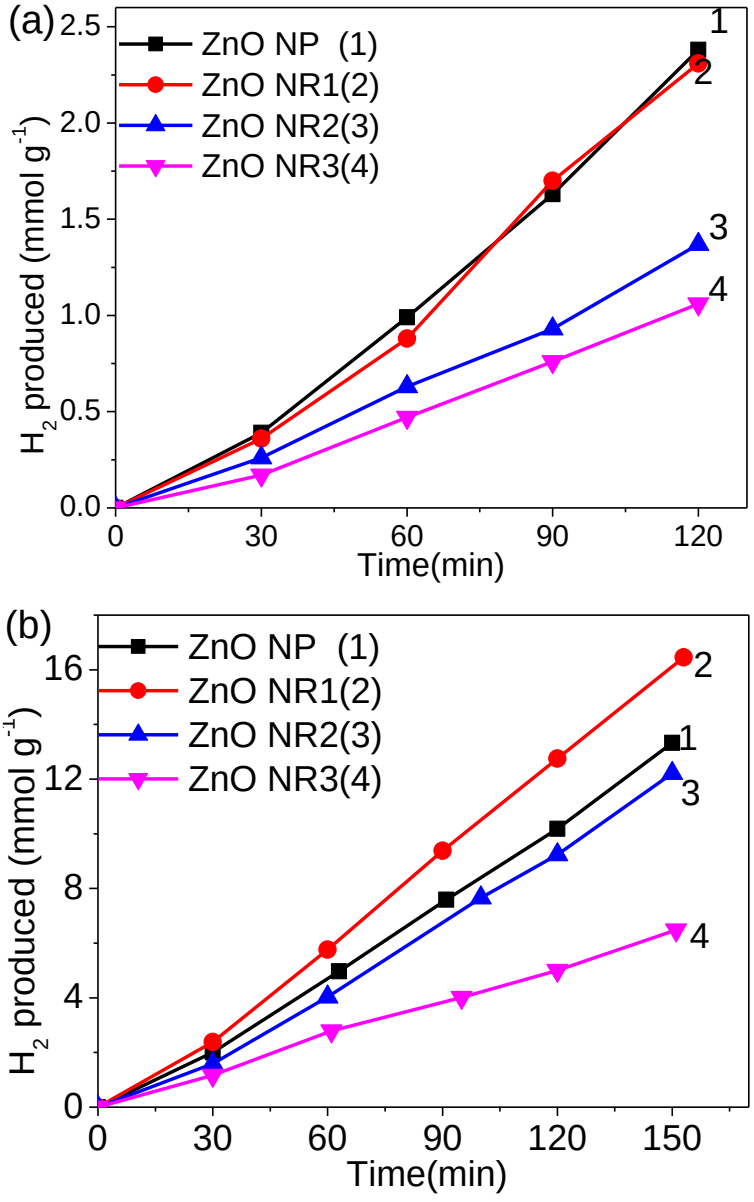


Fig. 5.5. Photocatalytic activity of (a) ZnO/CdS, (b) ZnO/Pt/CdS heterostructures employing different ZnO nanostructures.

heterostructures with ZnO NP, ZnO NR1, ZnO NR2, and ZNO NR3 are 1.32, 1.31, 0.68, and 0.59 mmol $h^{-1}g^{-1}$ respectively. We observe that the photocatalytic $H_2$ evolution rate from these heterostructures is in the trend of the BET surface areas of the ZnO nanostructures. ZnO NPs with the highest surface area (45.3 $m^2/g$) shows the highest photocatalytic activity, whereas ZnO NR3 with the least surface area (8.7 $m^2/g$), shows the least photocatalytic activity. Photocatalytic activity of ZnO NR1 and ZnO NR2 are also in the order of their BET surface areas. Similar to $TiO_2$ here also we observe significant increase in the photocatalytic activity of in presence of Pt nanoparticles. Fig. 5.5b shows the photocatalytic hydrogen evolution activity of ZnO/Pt/CdS heterostructures. The highest $H_2$ evolution (6.88 mmol $h^{-1}$ $g^{-1}$) is found with ZnO NR1 and the least (2.55 mmol $h^{-1}g^{-1}$) with ZnO NR3. We see that the photocatalytic $H_2$ evolution rate follows the trend in the BET surface areas of ZnO nanostructures (Fig. 5.6).

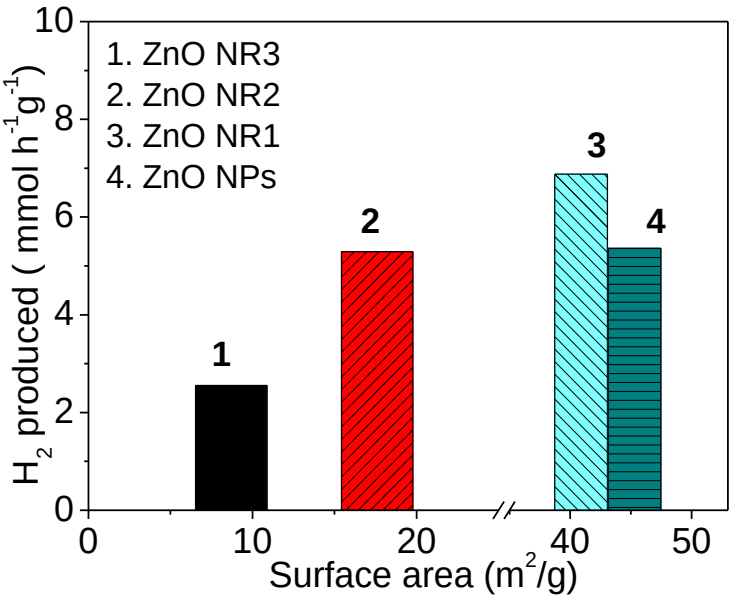


Fig. 5.6. Photocatalytic $H_2$ evolution from ZnO/Pt/CdS heterostructures.

The charge transfer process is believed to follow vectorial transfer of photoexcited electrons from CdS to ZnO (or $TiO_2$), as pointed out in the previous study from our lab [57]. Upon visible light irradiation, CdS gets excited and generates electron-hole pairs. The electron quickly migrates to CB of ZnO (or $TiO_2$) due to their suitable band alignment, which subsequently takes part in redox reaction, see Fig. 5.7.

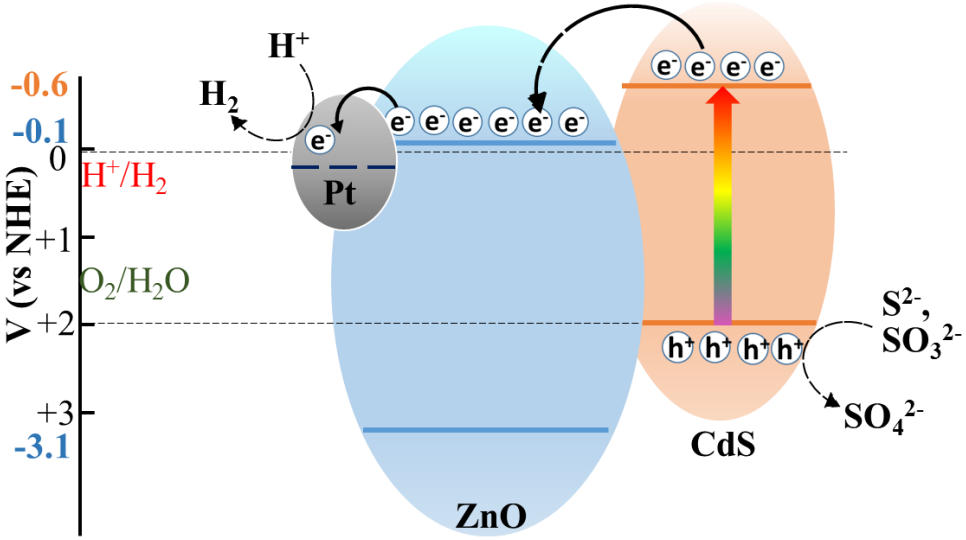


Fig. 5.7. Charge transfer process in ZnO/Pt/CdS heterostructure.
Figure adapted from [54].

## 5.4 Conclusions

In conclusion, the significant effect of morphology of the oxide nanostructures on visible light induced hydrogen evolution from $TiO_2/Cd_{0.8}Zn_{0.2}S$, $TiO_2/Pt/Cd_{0.8}Zn_{0.2}S$, ZnO/CdS, and ZnO/Pt/CdS heterostructures has been investigated. The effect of morphology and surface area to the photocatalytic activity has been observed, as expected. Among all $TiO_2$ nanostructures, $H_2Ti_3O_7$ nanotubes show highest photocatalytic hydrogen generation whereas $TiO_2$ powder (Degussa P-25) shows least photocatalytic hydrogen generation. ZnO/Pt/CdS heterostructures with ZnO nanorods1 shows the highest photocatalytic $H_2$ generation whereas those with ZnO nanorods3 show least $H_2$ generation. Photocatalytic activities of all these heterostructures generally follow the trend in the BET surface areas of the oxide nanostructures.

# Chapter 6

## In search of a new cocatalyst: Rhenium (VI) trioxide ($ReO_3$) for hydrogen generation on metal oxide based heterostructures.

*Loading cocatalyst on photocatalyst surface is being practiced regularly for improvement in hydrogen generation. Most common photocatalysts are noble metals, e.g., Pt. Rhenium (VI) trioxide, $ReO_3$ has been found to possess astonishingly high metallic character, with conductivity comparable to copper. Hence we thought, that $ReO_3$ can replace the metallic Pt cocatalyst in semiconductor heterostructures, such as, ZnO/Pt/CdS or $TiO_2$/Pt/CdS. $ReO_3$ nanoparticles was successfully prepared insitu to deposit on ZnO and $TiO_2$ surface. But ZnO($TiO_2$)/ $ReO_3$ heterostructure is found to be unstable in water and so could not be used in photocatalytic water splitting.*

# 6.1 Introduction

## 6.1.1 Need of Surface modification

In previous chapters, the effect of quantity of surface (area) of photocatalyst semiconductor particulate has been discussed, which actually facilitates step iii, i.e. surface chemical reaction of water splitting. More important aspect for this step is surface character, i.e., active sites. The photoexcited electrons and holes will lead to recombination, even if they get thermodynamically sufficient potentials for water splitting, if there are no active sites for redox reactions are available at the surface, where charge transport occurs. This stage, can be facilitated by the presence of a cocatalyst. Typically, the cocatalysts are noble metals, e.g., Pt, Au, Ag, Pd, Rh; or transition metals(oxides), e.g., Ni, Cu, $NiO_x$, $RuO_2$; and is decorated onto the surface of the photocatalyst as dispersed nanoparticles of few nm in size.

## 6.1.2 Role of Cocatalyst

Loading of cocatalyst significantly improves the $H_2$ evolution activity. The cocatalysts play pivotal roles: (a) Cocatalysts can bring down the activation potential for $H_2$ or $O_2$ generation reactions on the surface of semiconductors. Various studies suggests, that metal species deposited on semiconductors shifts the Fermi Level, lowering down it to significantly negative energy potentials. This shift improves the interfacial charge transfer process efficiency [58]. (b) Photoexcited electrons in the CB get shuttled to the cocatalyst and are thus separates from holes, by forming a Schottky barrier at the interface. As depicted in Fig. 6.1, the photoexcited electrons in the CB of a photocatalyst get migrated to $H_2$ evolution cocatalyst (process i) and reduce protons to $H_2$ (process ii), whereas the photoexcited holes left in the VB diffuse to the $O_2$ evolution cocatalyst and oxidize $H_2O$ to give $O_2$. (c) Cocatalysts can inhibit the photocorrosion and increase the stability of photocatalysts by trapping the photogenerated holes for $O_2$ evolution.

## 6.1.3 Pt-free cocatalyst

Particularly, the structural properties, as well as the intrinsic catalytic characteristics of a cocatalyst for gas evolution are of interest. For instance, Pt is a

well-known to exhibit excellent cocatalytic activity for $H_2$ evolution. However, it is not that a Pt loaded photocatalyst always exhibits the superior reactivity among other cocatalyst-loaded analogs. Hence, it can be concluded that the contribution of process (I) can be more important than that of process (II). For example, TaON loaded with Ru shows greater activity for $H_2$ evolution from aqueous solution of alcohol than Pt-TaON [59].

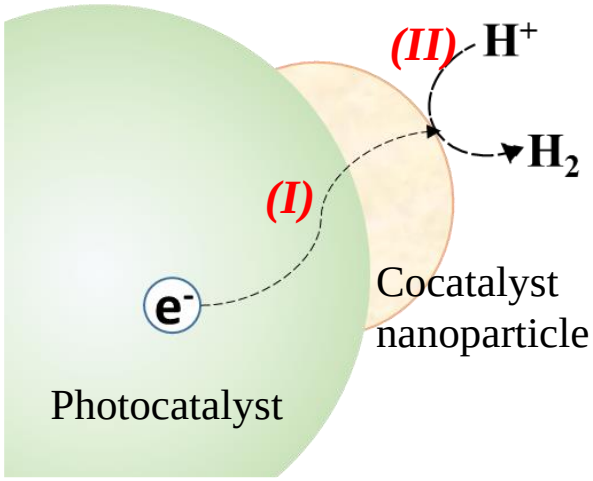


Fig. 6.1. Role of cocatalyst in photocatalytic water splitting.

Although that various factors, like, work function and band-edge potential of the photocatalyst and the cocatalyst, has been reported to effect the efficiency of process (i), a systematic understanding is yet to be recorded. Regardless, both (i) and (ii) should be considered to architect an effective photocatalytic system.

### 6.1.4 Scope of the current project

In the current project, we would like to explore the possibility of using Rhenium (VI) trioxide ($ReO_3$) as a co-catalyst. Rao and co-workers had synthesized $ReO_3$ nanoparticles under solvothermal conditions [60]. The transition metal oxide $ReO_3$ has been found to be metallic with an astonishingly high conductivity comparable to that of copper, having an electrical conductivity $10^5\ \Omega^{-1}\ cm^{-1}$, at room temperature [61]. $ReO_3$ adopts a simple cubic perovskite ($ABO_3$) structure with a vacant A site at the center of a unit cell. This site allows proton intercalation and wide lattice motions of the $ReO_6$ octahedral. The $ReO_3$ surface reactivity catalyzes reactions with the air moisture, leading to proton intercalation in the near-surface layers and to the formation of disordered phases, resulting in substantial ionic conductivity. Due to its metallic nature, $ReO_3$ exhibits plasmon absorption band in visible and NIR region [60]. Recently, metallic cocatalyst, such as Au, has found to enhance photocatalytic activity by SPR effect induced by appropriate visible irradiation [62]. Hence, we considered to use $ReO_3$ nanoparticles as a cocatalyst instead of Pt. Three mechanisms has been proposed by which metal SPR can enhance the photoreactivity[63] and illustrated in

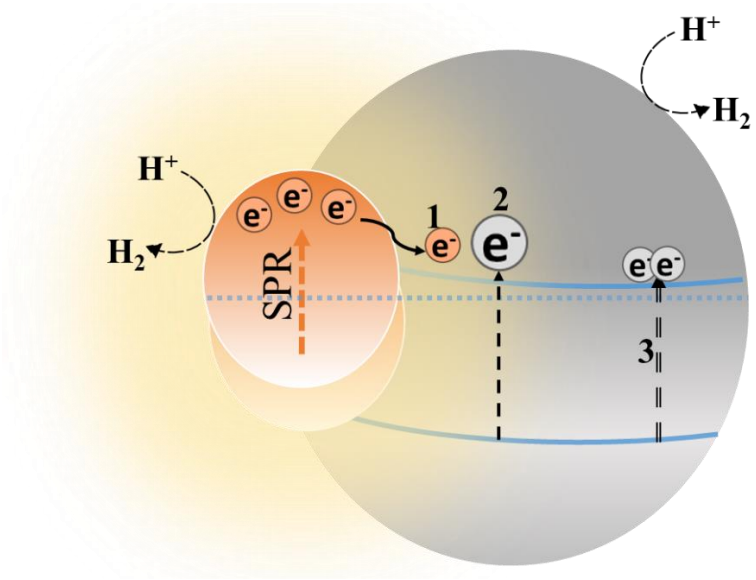


Fig 6.2. Mechanism of enhancement of photocatalytic activity in plasmonic-metal/semiconductor systems; (1) SPR induced charge transfer, (2) near-field induced boost in the energy intensity, and (3) scattering mechanism.

Fig 6.2. (1) SPR leads to the transfer of charge from photo-excited metal to the into the semiconductor surface, often termed the charge transfer mechanism. (2) near-field electromagnetic mechanism- Interaction of metal SPR with nearby semiconductor via an SPR-induced enhanced near-field, leading to increased charge carriers formation in the semiconductor. (3) So-called "scattering mechanism", the addition of metal nanoparticles does increase the extinction of the samples, effectively increasing the average photon pathlength. $ReO_3$ has also shown high catalytic reactivity in the photodegradation of methyl orange dye upon visible light irradiation [64]. We want to substitute the metallic part of $TiO_2$/Pt/CdS heterostructure and explore the photocatalytic activity of $TiO_2$/$ReO_3$/CdS heterostructure in water splitting.

## 6.2 Experimental Section

### 6.2.1 Synthesis of $ReO_3$ nanoparticles

250 mg Rhenium (VII) trioxide ($Re_2O_7$) and 2 mL of anhydrous 1, 4-dioxane were taken in a test tube, and was gently warmed in a water bath at 60°C for 6 h to obtain a colorless solution. The solution was cooled in an ice bath, and then the tube was taken out to allow the frozen mass to warm to RT. The $Re_2O_7$-dioxane complex (RDC) precipitated out as a dense pearl grey deposit. The freezing-melting operation was repeated to ensure complete separation of the complex. Then colorless supernatant liquid was decanted. The RDC complex was unstable in open air and was preserved as green ethanolic (10 mL) solution for later use.

To prepare $ReO_3$ NPs, 0.4 mL of this solution was taken along with 10 mL of toluene in a round bottom flask and was heated at 90°C oil bath with reflux for overnight while stirring. Blue colored $ReO_3$ NPs were precipitated out.

### 6.2.2 Preparation of $TiO_2/ReO_3$ heterostructure

0.3 mmol of $TiO_2$ was taken in a round bottom flask along with 20 mL toluene. Then the contents of the flask were sonicated for 5 mins. While sonicating, 0.4 mL of the $Re_2O_7$-dioxane solution was added to it dropwise and sonicated for 15 mins more. The flask was then kept in a 90°C oil bath for 2 hrs without condenser (to evaporate ethanol) with stirring. Then 10 mL of toluene was added and reflux was started and kept overnight. Blue colored $TiO_2/ReO_3$ heterostructure was precipitated and the product was centrifuged, washed with toluene, air dried and collected for further use.

## 6.3 Results and Discussion

Two $TiO_2$ based heterostructures were prepared successfully for water splitting: $TiO_2/ReO_3^{15\%}$ and $TiO_2/ReO_3^{7\%}$, the superscript denotes the mole percentage of $ReO_3$ with respect to $TiO_2$. Fig. 6.3 shows the absorption spectra of the samples. From the spectra we see, that the $TiO_2/ReO_3$ heterostructure can absorb in visible region, whereas $TiO_2$ only absorbs in UV region. Loading of $ReO_3$ can lead to an enhanced absorption. The absorption band at longer wavelengths originates from $ReO_3$ nano

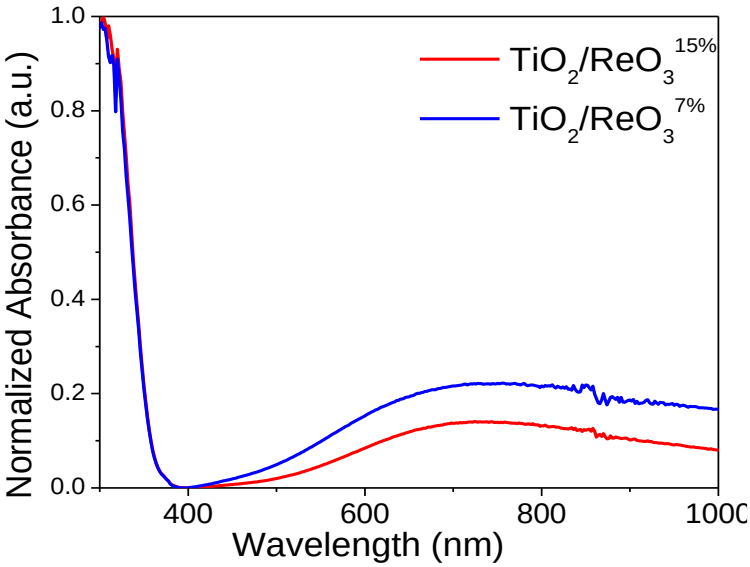


Fig. 6.3. Absorption spectra of $TiO_2/ReO_3$ heterostructures

particles, because $ReO_3$ is known to exhibit plasmon absorption band. This SPR band comes due to the metallic nature [60]. Fig. 6.4 shows the XRD spectra of $TiO_2/ReO_3$ heterostructures and it confirms the presence of rutile and anatase $TiO_2$.

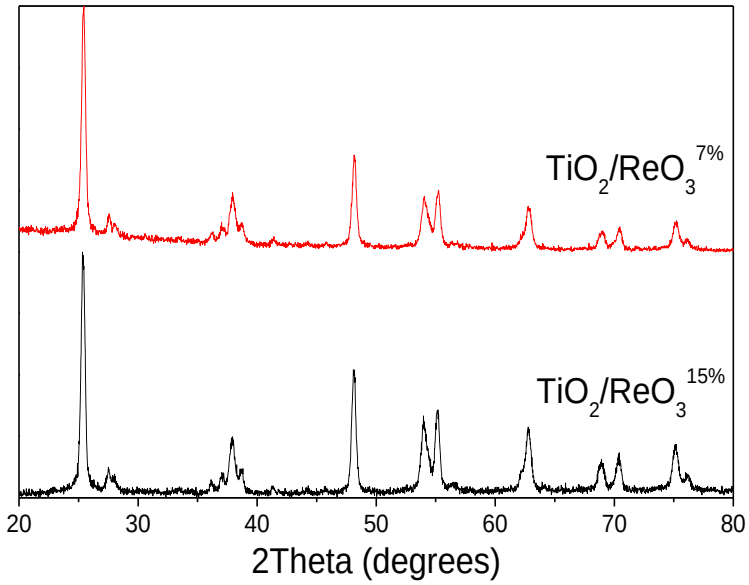


Fig. 6.4. PXRD patterns of $TiO_2/ReO_3$ heterostructures.

However, when the heterostructures was suspended in water, the bluish color of the heterostructures immediately disappeared and the solution became acidic, meaning that $ReO_3$ reacts with water, which has been observed sometime [65]. Hence, it is unstable in water and could not be used for water splitting.

## 6.4 Conclusion

$ReO_3$ has been tried to use as a cocatalyst for visible light driven water splitting. Besides possessing excellent metallic nature, $ReO_3$ is well-known for plasmonic absorbance in visible spectrum. Hence $ReO_3$ could be an ideal surface cocatalyst for the surface modification of wide band gap photocatalyst. $TiO_2/ReO_3$ heterostructure has been prepared successfully in this project. However, due to inherent instability of $ReO_3$ in water, we could not use $TiO_2/ReO_3$ for visible light driven water splitting. Nevertheless, the surface plasmon resonance on the metal-loaded photocatalysts can be an attractive way to utilize broader solar spectrum, especially for wide bandgap materials, such as $TiO_2$.

# Chapter 7

## To use Copper (II) Sulfide based Heterostructure for Visible Light driven Hydrogen generation

*To render visible light response in metal oxide photocatalyst, semiconductors with smaller band gap can be used to sensitize, as light harvesting antenna, in semiconductor heterostructures. In this project, we want to use CuS as a cocatalyst in ZnO($TiO_2$)/CuS heterostructures to employ in visible light driven photocatalytic water splitting. CuS was deposited in situ on ZnO($TiO_2$) to prepare the heterostructure and was used for $H_2$ generation. ZnO/CuZnS and ZnO/CuCdS heterostructures were also prepared for photocatalytic water splitting.*

# 7.1 Introduction

## 7.1.1 Aiming CdS-free Heterostructure

In previous chapters, successful visible irradiation driven $H_2$ evolution by water splitting on doped CdS and CdS sensitized metal oxides, has been demonstrated. However, this study, at the same time, raises concern over toxicity issue, of CdS, and same for other common sensitizers- CdSe, PbS etc. Also, sometimes very scarce and expensive Pt has been used as cocatalyst. An unsuccessful attempt, to employ $ReO_3$ as a cocatalyst, is also made. But $ReO_3$ is also very scarce. Hence, we considered, to look for a new CdS -free inexpensive plentiful cocatalyst, to use in the heterostructure involving metal oxides, for visible light driven water splitting.

Many kinds of new cocatalysts, using earth-abundant and cheap elements, have been demonstrated to facilitate photocatalytic water splitting in recent years. Transition metals, such as Co, Ni and Cu and transition metal oxides, e.g., $NiO_x$, $RuO_2$ have also been demonstrated as cocatalysts. Upon loading of these cocatalysts on the semiconductor particulates, a Schottky barrier forms at the interface of metal and semiconductor, which promotes charge separation. At the same time, these metals can catalyse the surface reaction to reduce the proton to $H_2$. Therefore, photocatalytic $H_2$ evolution activity can be enhanced if these metals are dispersed as cocatalysts on semiconductor particulate surface. Hence there is an ongoing effort to replace the noble metal cocatalysts and also some transition metal sulfides, such as, FeS, NiS, $NiS_2$, $MoS_2$, CuS, $MoS_3$ and $WS_2$, have been demonstrated as interesting alternative candidates for cost-efficient cocatalysts.

## 7.1.2 Scope of the current project

In this project we would like to use copper (II) sulphide as a visible light harvesting cocatalyst for water splitting. Very recently, a CuS/ZnS [66] and CuS/ZnO [67] photocatalysts, have been reported, and it is believed that this can facilitate the vectorial transfer of photoexcited electrons from the ZnS to CuS and hence, the charge separation improves and consequently the photocatalytic efficiency also enhances greatly. At the same time, this contact between CuS and ZnS is responsible for the photoinduced interfacial charge transfer (IFCT) from the valence band of the ZnS (or

ZnO) to the CuS, making the CuS/ZnS photocatalyst heterostructure active under the visible light irradiation, see Fig. 7.1. Hence, we considered to prepare ZnO/CuS heterostructures to study visible light driven water splitting. CuS, having a band gap of 2.2 eV [68], is visible light responsive, and ZnO/CuS could be a promising visible-light-active photocatalyst.

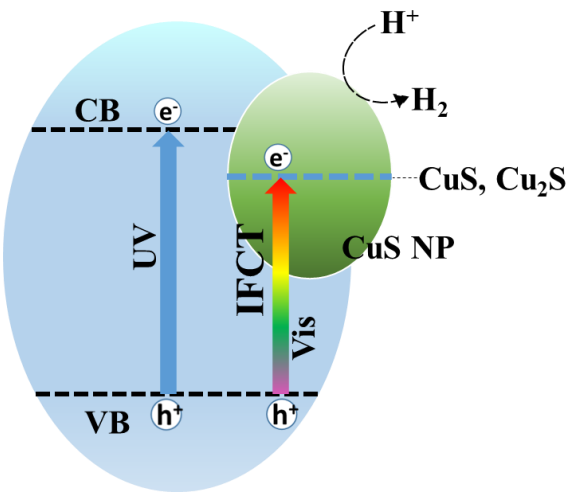


Fig. 7.1. Proposed charge transfer process from VB of ZnO to the CuS. Figure adapted from [66].

## 7.2 Experimental Section

### 7.2.1 Preparation of ZnO nanoparticles

In a typical preparation, 60 mL solution of 4 mmol zinc acetate dihydrate was taken in a round bottom flask and heated at 60°C with reflux and stirring. To this solution, 15 mL solution of 8 mmol KOH was added dropwise from the top of the condenser and refluxed for 2 hours more. The resulting white precipitate was centrifuged, washed with water and acetone and air dried at 60°C to get ZnO nanoparticles.

### 7.2.2 Preparation of ZnO/CuS heterostructures

To prepare ZnO/$(CuS)^{10\%}$ (superscript signifies that 10 mol% of CuS with respect to ZnO is deposited), 2 mmol of ZnO nanoparticles was added to 40 mL water and taken in a round bottom flask. The content was sonicated for 15 mins to get a dispersion of ZnO. Then 0.2 mmol copper (II) sulfate pentahydrate was added to it and kept for stirring using a magnetic stirrer for 20 mins. To this, a 10 mL solution of 0.4 mmol KOH was added dropwise and stirred for further 20 mins. Then a 20 mL solution of 0.2 mmol sodium sulfide was added to it dropwise while stirring and kept for further 20 mins. Then stirring stopped and the precipitate was centrifuged, washed with water and acetone and dried in open air to collect the ZnO/$(CuS)^{10\%}$ product. ZnO/$(CuS)^{20\%}$

and ZnO/$(CuS)^{30\%}$ was prepared in similar fashion while taking care of the Copper(II) sulfate pentahydrate, KOH and $Na_2S$ concentration.

### 7.2.3 Preparation of ZnO/CuZnS(CuCdS) heterostructures

ZnO/$(Cu_{0.7}Zn_{0.3}S)^{20\%}$ and ZnO/$(Cu_{0.7}Zn_{0.3}S)^{20\%}$ was prepared in in the same fashion as ZnO/CuS preparation, only required amount of zinc acetate dihydrate (or cadmium acetate dihydrate in case of ZnO/$(Cu_{0.7}Cd_{0.3}S)^{20\%}$ and ZnO/$(Cu_{0.7}Cd_{0.3}S)^{20\%}$ was taken along with copper sulfate pentahydrate.

## 7.3. Results and discussion

### 7.3.1 Characterizations of the Heterostructures

The absorption property of the ZnO/CuS heterostructure was observed and shown in Fig. 7.2. ZnO being a wide band gap semiconductor, only absorbs in UV region, but combining with CuS extends its absorption in the visible range.

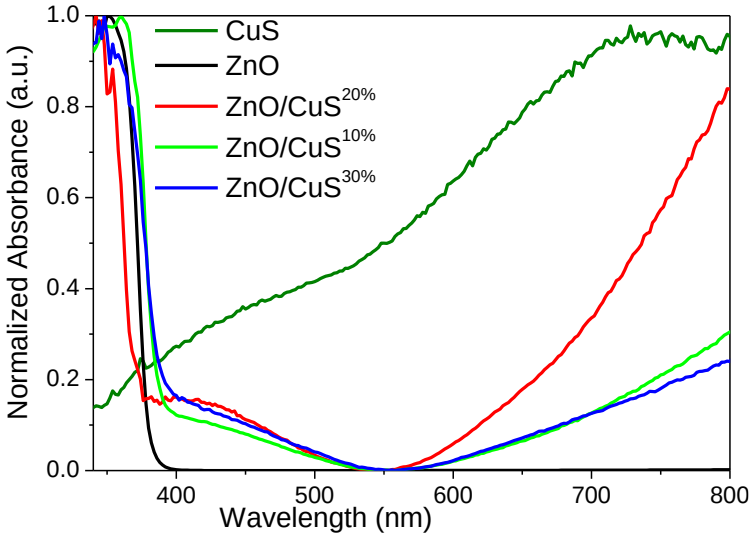


Fig. 7.2. Absorption spectra of ZnO/CuS heterostructures.

XRD patterns also confirms presence of hexagonal ZnO in the heterostructures, see Fig. 7.3a. ZnO/$(Cu_{0.7}Zn_{0.3}S)^{20\%}$ and ZnO/$(Cu_{0.7}Zn_{0.3}S)^{20\%}$ was also prepared and absorption spectra is shown in Fig. 7.3b and Fig. 7.3c.

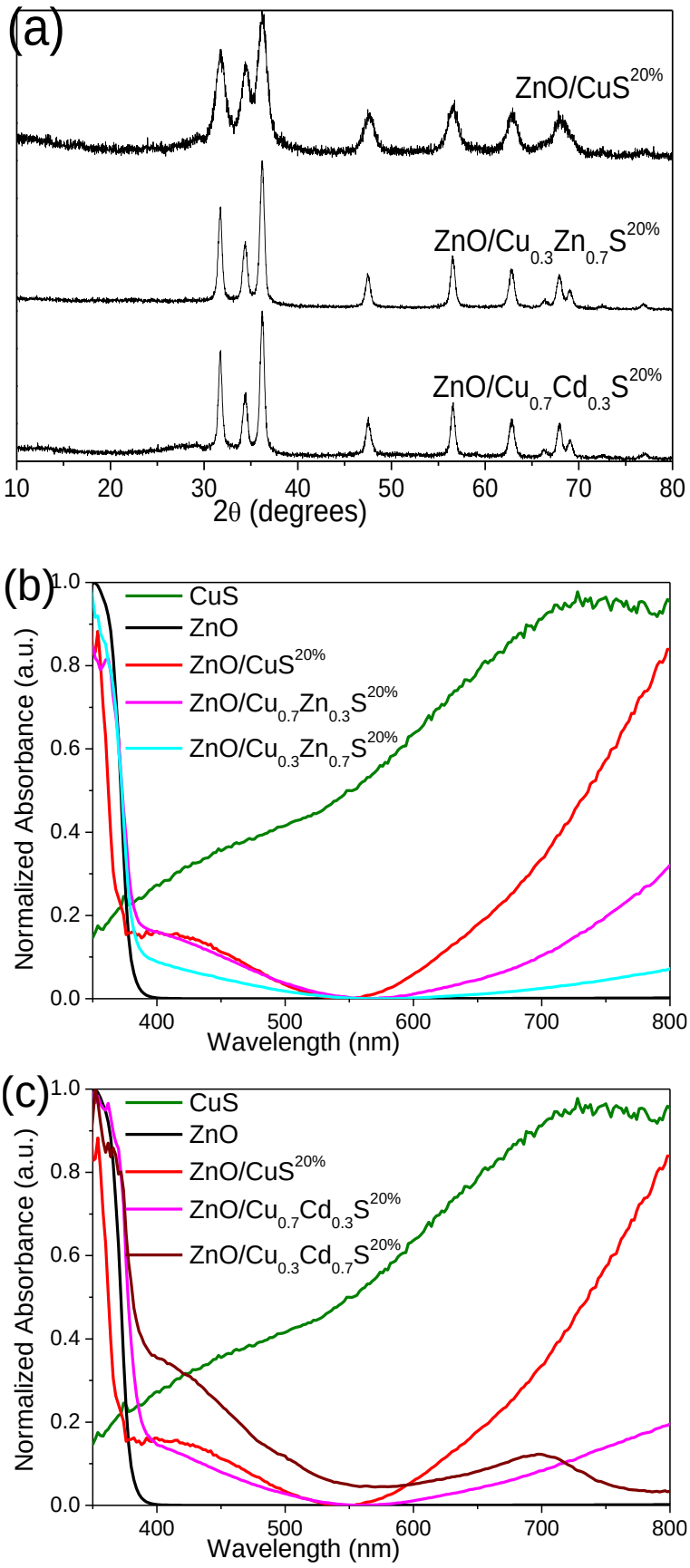


Fig. 7.3. (a) XRD patterns of ZnO/CuS, (b) Absorption spectra of ZnO/CuZnS, and (c) Absorption spectra of ZnO/CuCdS heterostructures.

### 7.3.2 Photocatalytic activity of ZnO/CuS haterostructures

To investigate photocatalytic efficiency, ZnO/CuS haterostructures with 10, 20 and 30 mol% were prepared and were subjected to visible light driven $H_2$ generation in presence of $Na_2S/Na_2SO_3$ sacrificial reagent. The results are shown in Fig. 7.4. Highest activity is seen with 10 mol% CuS, 12 µmol $g^{-1}$ $h^{-1}$. With increasing CuS content the activity decreases and 30 mol% CuS does not show any activity, which might happen, since beyond optimum concentration of cocatalyst, photocatalytic activity of the base photocatalyst decreases [9].

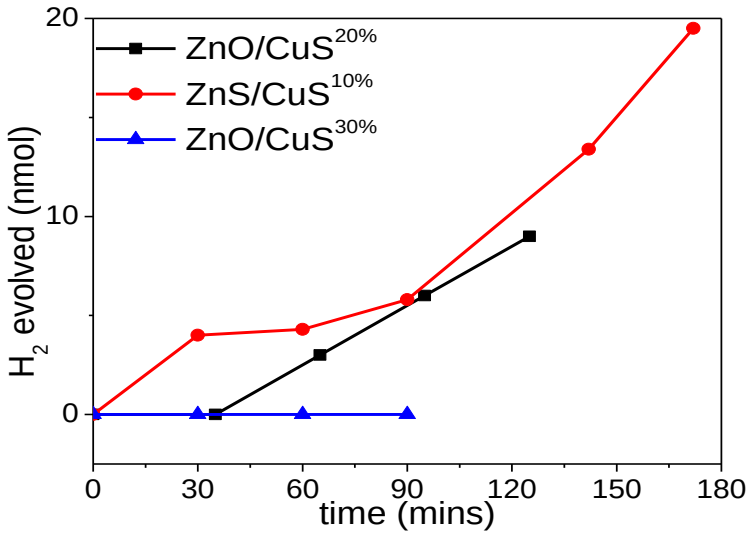


Fig. 7.4. Photocatalytic H2 evolution of ZnO/ CuS heterostructures.

Substitution of Cd with Zn leads to better efficiency in ZnO/CdZnS [57]. Hence ZnO/CuZnS and ZnO/CuCdS heterostructures were prepared. The photocatalytic $H_2$ evolution activities under visible light are shown in Fig. 7.5.

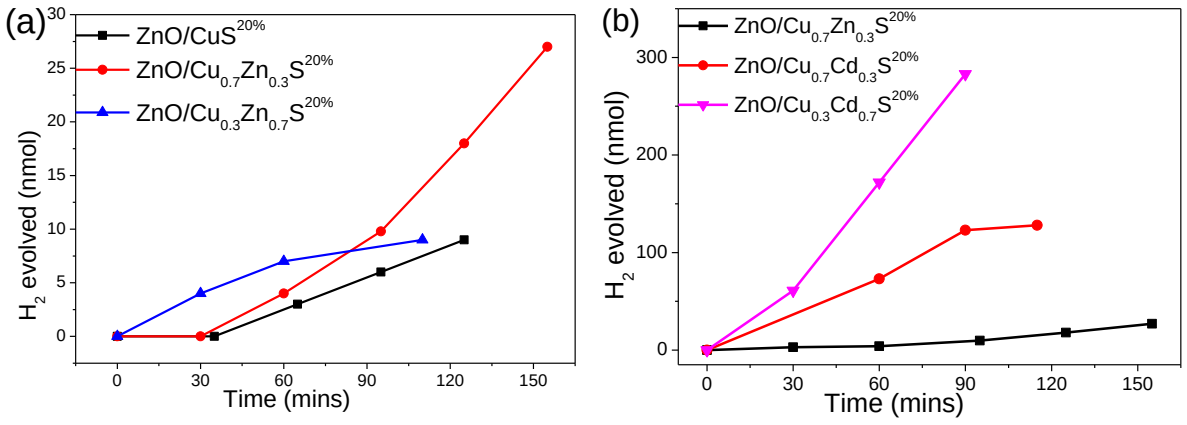


Fig. 7.5. $H_2$ evolution by (a) ZnO/CuZnS, (b) ZnO/CuCdS heterostructures.

Here we see that replacing Cu with Zn in CuS improves the $H_2$ evolution efficiency, but not much, Fig. 7.5a, whereas replacing with Cd, i.e., ZnO/CuCdS heterostructure, improves hugely, see Fig. 7.5b.

## 7.4 Conclusion

ZnO/CuS haterostructures were prepared in simple solution process. Photocatalytic $H_2$ evolution by ZnO/CuS haterostructures, has been attempted. The heterostructures show photocatalytic activity under visible light irradiation, however, the activity is very mild. Nevertheless, there are rooms for improvement, and CuS could be very efficient photocatalyst. Better preparation method might help, because, in general the loading method of the cocatalyst effects the photocatalytic activity [9], as this determines the physicochemical characteristics of the loaded cocatalyst, e.g., valence state, dispersion etc. This work shows a possibility for replacing noble metal and toxic cocatalysts by economical CuS for photocatalytic $H_2$ production.

# Chapter 8
# Conclusions of the Dissertation

As fossil fuels are likely to be depleted in the near future, the utilization of solar energy to produce $H_2$ from water using semiconductor photocatalysts has been considered as the most plausible solution. Upon irradiation with light, the semiconductor absorbs photon having energy exceeding the band gap, generating electron-hole pair. Immediately charge separation happens and the electrons migrate to the surface to take part in redox reaction to produce $H_2$. In application to energy conversion, it is most important to find semiconductor with a suitable band structure, the band gap must straddle the reduction and oxidation potentials of water to produce $H_2$ by water splitting. Indeed, a group of successful photocatalysts for water splitting has been explored, comprised based of metal oxide systems mainly, such as $TiO_2$, ZnS, ZnO etc., only active under UV irradiation although, due to their wide band gap. Hence, to extend the photocatalytic activity under visible light irradiation, appropriate band engineering is needed, as practiced in the current project. Several strategies have been adopted to modify the UV-active wide bandgap semiconductors, such as doping, preparing solid solutions, constructing heterostructures, plasmonic modification and loading cocatalyst and discussed in this dissertation.

Firstly, anion doping in metal sulfides has been done successfully. P,Cl- and N,F- cosubstitution has led to visible light response in ZnS (and CdS), due to creation of mid gap energy level, effectively reducing the energy gap. Such cosubstitution in CdS has brought about tremendous enhancement in photocatalytic activity under visible light irradiation, which might improve other application as well.

Secondly, in order to bring visible light activity, ZnO was alloyed with narrow band gap semiconductor CdO. A series of $Zn_{1-x}Cd_xO$ solid solution, x= 0, 0.2, 0.4, 0.6, 0.8, 1, were prepared successfully and confirmed by XRD. Absorption spectra also showed desired band gap narrowing. However, ZnCdO did not show any improvement in $H_2$ generation activity, rather activity decreased with increasing Cd content in $Zn_{1-x}Cd_xO/CdS^{20\%}$ photocatalyst.

Thirdly, to bring visible light activity in $TiO_2$ and ZnO, heterostructures were prepared. ZnO($TiO_2$)/CdS and ZnO($TiO_2$)/Pt/CdS shows excellent photocatalytic activity. The dependence of activity on morphology and surface area has been demonstrated, which confirms that the morphology with highest surface area, such as nanotubes, possesses the highest activity and lowest surface area gives the least activity, such as for nanoparticles.

Fourthly, loading plasmonic metal as a cocatalyst induces visible light activity. Hence $ReO_3$ loaded $TiO_2$ heterostructures were prepared successfully, which absorb in visible region, due to SPR of $ReO_3$. However, $TiO_2$/ $ReO_3$ is found to be unstable in water and hence could not be used in water splitting.

Lastly, in search of a Pt and CdS free cocatalyst, CuS was used in such purpose. ZnO/CuS and ZnO/$Cu_{1-x}Zn_xS$ heterostructures prepared successfully and used for visible light driven water splitting. The heterostructures had showed mild activity towards $H_2$ generation. Nevertheless, CuS showed promise to act as a visible light active hydrogen evolution cocatalyst.

Thus, the works presented in this dissertation shed some light on the continuous efforts by the community for efficient visible (sun)light responsive photocatalyst. Although, current photocatalytic systems are far away from practical utilization, an estimation suggests that 10000 5km x 5km solar photocatalyst plants (~1% of the earth's desert area) with a energy conversion efficiency of 10%, would be sufficient to supply one-third of the projected energy needs in 2050 from solar energy [6]. Nevertheless, In future, the research on photocatalytic water splitting, is expected to not only looking for new semiconductor photocatalyst and cocatalyst materials and improving their synthesis process, but also finding inexpensiveness, abundance and non-toxicity of the base photocatalysts and cocatalyst will become important, as pointed out in this dissertation.

# List of References


[1] A. Fujishima and K. Honda, “Electrochemical Photolysis of Water at a Semiconductor Electrode,” *Nature*, vol. 238, no. 5358, pp. 37–38, Jul. 1972.

[2] K. Fujihara, T. Ohno, and M. Matsumura, “Splitting of water by electrochemical combination of two photocatalytic reactions on TiO2 particles,” *J. Chem. Soc. Faraday Trans.*, vol. 94, no. 24, pp. 3705–3709, Jan. 1998.

[3] K. Sayama and H. Arakawa, “Effect of Na2CO3 addition on photocatalytic decomposition of liquid water over various semiconductor catalysis,” *J. Photochem. Photobiol. A Chem.*, vol. 77, no. 2–3, pp. 243–247, Jan. 1994.

[4] M. Hara, T. Kondo, M. Komoda, S. Ikeda, K. Shinohara, and A. Tanaka, “RuO2-Loaded β-Ge3N4 as a Non-Oxide Photocatalyst for Overall Water Splitting,” vol. 2, pp. 357–358, 1998.

[5] Y. Inoue, “Photocatalytic water splitting by RuO2- loaded metal oxides and nitrides with d0- and d10- related electronic configurations,” *Energy Environ. Sci.*, vol. 2, p. 364, 2009.

[6] K. Maeda and K. Domen, “Photocatalytic water splitting: Recent progress and future challenges,” *J. Phys. Chem. Lett.*, vol. 1, pp. 2655–2661, 2010.

[7] A. Kudo and Y. Miseki, “Heterogeneous photocatalyst materials for water splitting,” *Chem. Soc. Rev. IMPORTANT*, vol. 38, no. 1, pp. 253–278, 2009.

[8] T. Ikeda, T. Nomoto, K. Eda, Y. Mizutani, H. Kato, A. Kudo, and H. Onishi, “Photoinduced Dynamics of TiO2 Doped with Cr and Sb,” *J. Phys. Chem. C*, vol. 112, no. 4, pp. 1167–1173, Jan. 2008.

[9] K. Maeda, “Photocatalytic water splitting using semiconductor particles: History and recent developments,” *J. Photochem. Photobiol. C Photochem. Rev.*, vol. 12, no. 4, pp. 237–268, Dec. 2011.

[10] J. J. Loferski, “Theoretical Considerations Governing the Choice of the Optimum Semiconductor for Photovoltaic Solar Energy Conversion,” *J. Appl. Phys.*, vol. 27, no. 7, p. 777, May 1956.

[11] T. Aramoto, S. Kumazawa, H. Higuchi, T. Arita, S. Shibutani, T. Nishio, J. Nakajima, M. Tsuji, A. Hanafusa, T. Hibino, K. Omura, H. Ohyama, and M. Murozono, “16.0% Efficient Thin-Film CdS/CdTe Solar Cells,” *Jpn. J. Appl. Phys.*, vol. 36, no. Part 1, No. 10, pp. 6304–6305, Oct. 1997.

[12] A. Morales-Acevedo, “Can we improve the record efficiency of CdS/CdTe solar cells?,” *Sol. Energy Mater. Sol. Cells*, vol. 90, no. 15, pp. 2213–2220, Sep. 2006.

[13] R. W. Miles, K. M. Hynes, and I. Forbes, “Photovoltaic solar cells: An overview of state-of-the-art cell development and environmental issues,” *Prog. Cryst. Growth Charact. Mater.*, vol. 51, no. 1–3, pp. 1–42, Jan. 2005.

[14] R. Asahi, T. Morikawa, T. Ohwaki, K. Aoki, and Y. Taga, “Visible-Light Photocatalysis in Nitrogen-Doped Titanium Oxides,” *Science (80-. ).*, vol. 293, no. July, pp. 269–271, 2001.

[15] R. Saha, S. Revoju, V. I. Hegde, U. V Waghmare, a Sundaresan, and C. N. R. Rao, “Remarkable properties of ZnO heavily substituted with nitrogen and fluorine, ZnO(1-x)(N,F)x.,” *Chemphyschem*, vol. 14, no. 12, pp. 2672–7, Aug. 2013.

[16] N. Kumar, U. Maitra, V. I. Hegde, U. V Waghmare, A. Sundaresan, and C. N. R. Rao, “Synthesis, characterization, photocatalysis, and varied properties of TiO2 cosubstituted with nitrogen and fluorine.,” *Inorg. Chem.*, vol. 52, no. 18, pp. 10512–9, Sep. 2013.

[17] A. H. Rubel and J. Podder, “Structural and Electrical Transport Properties of CdS and Al-doped CdS Thin Films Deposited by Spray Pyrolysis,” *J. Sci. Res.*, vol. 4, no. 1, p. 11, Dec. 2011.

[18] D. Wu, Y. Jiang, Y. Yu, Y. Zhang, G. Li, Z. Zhu, C. Wu, L. Wang, L. Luo, and J. Jie, “Nonvolatile multibit Schottky memory based on single n-type Ga doped CdSe nanowires.,” *Nanotechnology*, vol. 23, no. 48, p. 485203, Dec. 2012.

[19] R. M. Ma, L. Dai, H. B. Huo, W. Q. Yang, G. G. Qin, P. H. Tan, C. H. Huang, and J. Zheng, “Synthesis of high quality n-type CdS nanobelts and their applications in nanodevices,” *Appl. Phys. Lett.*, vol. 89, no. 20, p. 203120, Nov. 2006.

[20] A. Podestà, N. Armani, G. Salviati, N. Romeo, A. Bosio, and M. Prato, “Influence of the fluorine doping on the optical properties of CdS thin films for photovoltaic applications,” *Thin Solid Films*, vol. 511–512, pp. 448–452, Jul. 2006.

[21] C. Wu, J. Jie, L. Wang, Y. Yu, Q. Peng, X. Zhang, J. Cai, H. Guo, D. Wu, and Y. Jiang, “Chlorine-doped n-type CdS nanowires with enhanced photoconductivity.,” *Nanotechnology*, vol. 21, no. 50, p. 505203, Dec. 2010.

[22] B. Wu, Y. Jiang, D. Wu, S. Li, L. Wang, Y. Yu, Z. Wang, and J. Jie, “Nitrogen Doped n-Type CdS Nanoribbons with Tunable Electrical and Photoelectrical Properties,” *J. Nanosci. Nanotechnol.*, vol. 11, no. 3, pp. 2003–2011, Mar. 2011.

[23] Y. Wang, Y. Jiang, D. Wu, Y. Sheng, L. Chen, G. Li, and J. Jie, “Field Effect Properties of Phosphorus Doped CdS Single-Crystal Nanoribbon via Co-Thermal-Evaporation,” *J. Nanosci. Nanotechnol.*, vol. 10, no. 1, pp. 433–439, Jan. 2010.

[24] L. P. Deshmukh, A. B. Palwe, and V. S. Sawant, “An investigation of arsenic-doped CdS/electrolyte solar cells,” *Sol. Cells*, vol. 28, no. 1, pp. 1–10, Jan. 1990.

[25] Q. Peng, J. Jie, C. Xie, L. Wang, X. Zhang, D. Wu, Y. Yu, C. Wu, Z. Wang, and P. Jiang, “Nano-Schottky barrier diodes based on Sb-doped ZnS nanoribbons with controlled p-type conductivity,” *Appl. Phys. Lett.*, vol. 98, no. 12, p. 123117, 2011.

[26] C. Wu, L. Wang, Z. Zhang, X. Zhang, Q. Peng, J. Cai, Y. Yu, H. Guo, and J. Jie, “Synthesis and optoelectronic properties of silver-doped n-type CdS nanoribbons,” *Front. Optoelectron. China*, vol. 4, no. 2, pp. 161–165, Jun. 2011.

[27] R. Tiwari, V. Dubey, and R. K. Tamrakar, “Copper Doped Cadmium Sulphide (CdS:Cu) Quantum Particles: Topological , Morphology and Photoluminescence Studies,” vol. 3, no. 3, pp. 67–74, 2013.

[28] G. Giribabu, D. A. Reddy, G. Murali, and R. P. Vijayalakshmi, “Structural and optical studies on Mg doped CdS nanoparticles by simple co-precipitation method,” in *Solid State Physics: Proceedings of The 57th DAE Solid State Physics Symposium 2012*, 2013, vol. 1512, no. 1, pp. 186–187.

[29] C. W. Na, D. S. Han, D. S. Kim, Y. J. Kang, J. Y. Lee, J. Park, D. K. Oh, K. S. Kim, and D. Kim, “Photoluminescence of Cd1-xMnxS (x < or = 0.3) nanowires.,” *J. Phys. Chem. B*, vol. 110, no. 13, pp. 6699–704, Apr. 2006.

[30] D. S. Kim, Y. J. Cho, J. Park, J. Yoon, Y. Jo, and M.-H. Jung, “(Mn, Zn) Co-Doped CdS Nanowires,” *J. Phys. Chem. C*, vol. 111, no. 29, pp. 10861–10868, Jul. 2007.

[31] G. Murali, D. Amaranatha Reddy, B. PoornaPrakash, R. P. Vijayalakshmi, B. K. Reddy, and R. Venugopal, “Room temperature magnetism of Fe doped CdS nanocrystals,” *Phys. B Condens. Matter*, vol. 407, no. 12, pp. 2084–2088, Jun. 2012.

[32] K. Kaur, G. S. Lotey, and N. K. Verma, “Structural, optical and magnetic properties of cobalt-doped CdS dilute magnetic semiconducting nanorods,” *Mater. Chem. Phys.*, vol. 143, no. 1, pp. 41–46, Dec. 2013.

[33] M. Elango, D. Nataraj, K. Prem Nazeer, and M. Thamilselvan, “Synthesis and characterization of nickel doped cadmium sulfide (CdS:Ni2+) nanoparticles,” *Mater. Res. Bull.*, vol. 47, no. 6, pp. 1533–1538, Jun. 2012.

[34] K. S. Kumar, A. Divya, and P. S. Reddy, “Synthesis and characterization of Cr doped CdS nanoparticles stabilized with polyvinylpyrrolidone,” *Appl. Surf. Sci.*, vol. 257, no. 22, pp. 9515–9518, Sep. 2011.

[35] P. Jiang, J. Jie, Y. Yu, Z. Wang, C. Xie, X. Zhang, C. Wu, L. Wang, Z. Zhu, and L. Luo, “Aluminium-doped n-type ZnS nanowires as high-performance UV and humidity sensors,” *J. Mater. Chem.*, vol. 22, no. 14, p. 6856, 2012.

[36] M.-Y. Lu, M.-P. Lu, Y.-A. Chung, M.-J. Chen, Z. L. Wang, and L.-J. Chen, “Intercrossed Sheet-Like Ga-Doped ZnS Nanostructures with Superb Photocatalytic Actvitiy and Photoresponse,” *J. Phys. Chem. C*, vol. 113, no. 29, pp. 12878–12882, Jul. 2009.

[37] B. Sotillo, P. Fernández, and J. Piqueras, “Cathodoluminescence of In doped ZnS nanostructures grown by vapor–solid method,” *J. Alloys Compd.*, vol. 563, pp. 113–118, Jun. 2013.

[38] T. Kucukomeroglu, E. Bacaksiz, C. Terzioglu, and A. Varilci, “Influence of fluorine doping on structural, electrical and optical properties of spray pyrolysis ZnS films,” *Thin Solid Films*, vol. 516, no. 10, pp. 2913–2916, Mar. 2008.

[39] Y. Yu, J. Jie, P. Jiang, L. Wang, C. Wu, Q. Peng, X. Zhang, Z. Wang, C. Xie, D. Wu, and Y. Jiang, “High-gain visible-blind UV photodetectors based on chlorine-doped n-type ZnS nanoribbons with tunable optoelectronic properties,” *J. Mater. Chem.*, vol. 21, no. 34, p. 12632, 2011.

[40] G. D. Yuan, W. J. Zhang, W. F. Zhang, X. Fan, I. Bello, C. S. Lee, and S. T. Lee, “p-type conduction in nitrogen-doped ZnS nanoribbons,” *Appl. Phys. Lett.*, vol. 93, no. 21, p. 213102, 2008.

[41] S. Zhang, H. Kinto, T. Yatabe, and S. Iida, “Nitrogen and phosphorus doping in ZnS layers grown by vapor phase epitaxy on GaAs substrates,” *J. Cryst. Growth*, vol. 86, no. 1–4, pp. 372–376, Jan. 1988.

[42] V. Ramasamy, K. Praba, and G. Murugadoss, “Synthesis and study of optical properties of transition metals doped ZnS nanoparticles.,” *Spectrochim. Acta. A. Mol. Biomol. Spectrosc.*, vol. 96, pp. 963–71, Oct. 2012.

[43] D. A. Reddy, D. H. Kim, S. J. Rhee, B. W. Lee, and C. Liu, “Tunable blue-green-emitting wurtzite ZnS:Mg nanosheet-assembled hierarchical spheres for near-UV white LEDs.,” *Nanoscale Res. Lett.*, vol. 9, no. 1, p. 20, Jan. 2014.

[44] P. V. Radovanovic, C. J. Barrelet, S. Gradečak, F. Qian, and C. M. Lieber, “General Synthesis of Manganese-Doped II−VI and III−V Semiconductor Nanowires,” *Nano Lett.*, vol. 5, no. 7, pp. 1407–1411, Jul. 2005.

[45] T. Kang, J. Sung, W. Shim, H. Moon, J. Cho, Y. Jo, W. Lee, and B. Kim, “Synthesis and Magnetic Properties of Single-Crystalline Mn/Fe-Doped and Co-doped ZnS Nanowires and Nanobelts,” *J. Phys. Chem. C*, vol. 113, no. 14, pp. 5352–5357, Apr. 2009.

[46] C. Bi, L. Pan, M. Xu, J. Yin, L. Qin, J. Liu, H. Zhu, and J. Q. Xiao, “Synthesis and characterization of Co-doped wurtzite ZnS nanocrystals,” *Mater. Chem. Phys.*, vol. 116, no. 2–3, pp. 363–367, Aug. 2009.

[47] H. Soni, M. Chawda, and D. Bodas, “Electrical and optical characteristics of Ni doped ZnS clusters,” *Mater. Lett.*, vol. 63, no. 9–10, pp. 767–769, Apr. 2009.

[48] D. Amaranatha Reddy, A. Divya, G. Murali, R. P. Vijayalakshmi, and B. K. Reddy, “Synthesis and optical properties of Cr doped ZnS nanoparticles capped by 2-mercaptoethanol,” *Phys. B Condens. Matter*, vol. 406, no. 10, pp. 1944–1949, May 2011.

[49] Y. Hong, J. Zhang, X. Wang, Y. Wang, Z. Lin, J. Yu, and F. Huang, “Influence of lattice integrity and phase composition on the photocatalytic hydrogen production efficiency of ZnS nanomaterials.,” *Nanoscale*, vol. 4, no. 9, pp. 2859–62, Apr. 2012.

[50] S. Xiong, B. Xi, C. Wang, D. Xu, X. Feng, Z. Zhu, and Y. Qian, “Tunable Synthesis of Various Wurtzite ZnS Architectural Structures and Their Photocatalytic Properties,” *Adv. Funct. Mater.*, vol. 17, no. 15, pp. 2728–2738, Oct. 2007.

[51] T. Hisatomi, J. Kubota, and K. Domen, “Recent advances in semiconductors for photocatalytic and photoelectrochemical water splitting,” *Chem. Soc. Rev.*, vol. 43, pp. 7520–7535, 2014.

[52] X. Wang, G. Liu, Z.-G. Chen, F. Li, L. Wang, G. Q. Lu, and H.-M. Cheng, “Enhanced photocatalytic hydrogen evolution by prolonging the lifetime of carriers in ZnO/CdS heterostructures.,” *Chem. Commun. (Camb).*, pp. 3452–3454, 2009.

[53] S. S. Srinivasan, J. Wade, and E. K. Stefanakos, “Visible Light Photocatalysis via CdS/TiO2 Nanocomposite Materials,” *J. Nanomater.*, vol. 2006, pp. 1–7, 2006.

[54] S. R. Lingampalli, U. K. Gautam, and C. N. R. Rao, “Highly efficient photocatalytic hydrogen generation by solution-processed ZnO/Pt/CdS, ZnO/Pt/Cd1−xZnxS and ZnO/Pt/CdS1−xSex hybrid nanostructures,” *Energy Environ. Sci.*, vol. 6, no. 12, p. 3589, 2013.

[55] S. K. Choi, S. Kim, S. K. Lim, and H. Park, “Photocatalytic Comparison of TiO2 Nanoparticles and Electrospun TiO2 Nanofibers: Effects of Mesoporosity and Interparticle Charge Transfer,” *J. Phys. Chem. C*, vol. 114, no. 39, pp. 16475–16480, Oct. 2010.

[56] A. McLaren, T. Valdes-Solis, G. Li, and S. C. Tsang, “Shape and size effects of ZnO nanocrystals on photocatalytic activity.,” *J. Am. Chem. Soc.*, vol. 131, no. 35, pp. 12540–1, Sep. 2009.

[57] S. R. Lingampalli, U. K. Gautam, and C. N. R. Rao, “Highly efficient photocatalytic hydrogen generation by solution-processed ZnO/Pt/CdS, ZnO/Pt/Cd1−xZnxS and ZnO/Pt/CdS1−xSex hybrid nanostructures,” *Energy Environ. Sci.*, vol. 6, no. 12, p. 3589, Nov. 2013.

[58] E. Kowalska, H. Remita, C. Colbeau-Justin, J. Hupka, and J. Belloni, “Modification of Titanium Dioxide with Platinum Ions and Clusters: Application in Photocatalysis,” *J. Phys. Chem. C*, vol. 112, no. 4, pp. 1124–1131, Jan. 2008.

[59] M. Hara, J. Nunoshige, T. Takata, J. N. Kondo, and K. Domen, “Unusual enhancement of H2 evolution by Ru on TaON photocatalyst under visible light irradiation.,” *Chem. Commun. (Camb).*, pp. 3000–3001, 2003.

[60] K. Biswas and C. N. R. Rao, “Metallic ReO3 nanoparticles.,” *J. Phys. Chem. B*, vol. 110, no. 2, pp. 842–5, Jan. 2006.

[61] A. Ferretti, D. B. Rogers, and J. B. Goodenough, “The relation of the electrical conductivity in single crystals of rhenium trioxide to the conductivities of Sr2MgReO6 and NaxWO3,” *J. Phys. Chem. Solids*, vol. 26, no. 12, pp. 2007–2011, Dec. 1965.

[62] J.-J. Chen, J. C. S. Wu, P. C. Wu, and D. P. Tsai, “Plasmonic Photocatalyst for H2 Evolution in Photocatalytic Water Splitting,” *J. Phys. Chem. C*, vol. 115, no. 1, pp. 210–216, Jan. 2011.

[63] S. Linic, P. Christopher, and D. B. Ingram, “Plasmonic-metal nanostructures for efficient conversion of solar to chemical energy,” *Nat. Mater.*, vol. 10, no. 12, pp. 911–921, 2011.

[64] Y. Y. Chong and W. Y. Fan, “Facile synthesis of single crystalline rhenium (VI) trioxide nanocubes with high catalytic efficiency for photodegradation of methyl orange.,” *J. Colloid Interface Sci.*, vol. 397, pp. 18–23, May 2013.

[65] E. Cazzanelli, M. Castriota, S. Marino, N. Scaramuzza, J. Purans, A. Kuzmin, R. Kalendarev, G. Mariotto, and G. Das, “Characterization of rhenium oxide films and their application to liquid crystal cells: RXN WITH WATER,” *J. Appl. Phys.*, vol. 105, pp. 1–7, 2009.

[66] J. Zhang, J. Yu, Y. Zhang, Q. Li, and J. R. Gong, “Visible Light Photocatalytic H2- Production Activity of CuS/ZnS Porous Nanosheets Based on Photoinduced Interfacial Charge Transfer,” pp. 4774–4779, 2011.

[67] M. Lee and K. Yong, “Highly efficient visible light photocatalysis of novel CuS/ZnO heterostructure nanowire arrays,” *Nanotechnology*, vol. 23, p. 194014, 2012.

[68] J. Yu, J. Zhang, and S. Liu, “Ion-exchange synthesis and enhanced visible-light photoactivity of CuS/ZnS nanocomposite hollow spheres,” *J. Phys. Chem. C*, vol. 114, pp. 13642–13649, 2010.